

**Design of highly efficient NO<sub>x</sub> storage-reduction catalysts from  
layered double hydroxides for NO<sub>x</sub> emission control from  
naphtha cracker flue gases**

Ruoyan Yang,<sup>1</sup> Yuhua Cui,<sup>1</sup> Qinghua Yan,<sup>1</sup> Cheng Zhang,<sup>1</sup> Lei Qiu,<sup>1</sup> Dermot O'Hare,<sup>2</sup>

Qiang Wang<sup>1,\*</sup>

<sup>1</sup>College of Environmental Science and Engineering, Beijing Forestry University, 35  
Qinghua East Road, Haidian District, Beijing 100083, P. R. China

<sup>2</sup>Chemistry Research Laboratory, Department of Chemistry, University of Oxford, 12  
Mansfield Road, Oxford, OX1 3TA, UK

\*Corresponding author:

College of Environmental Science and Engineering, Beijing Forestry University, 35  
Qinghua East Road, Haidian District, Beijing 100083, China

E-mail: [qiang.wang.ox@gmail.com](mailto:qiang.wang.ox@gmail.com); [qiangwang@bjfu.edu.cn](mailto:qiangwang@bjfu.edu.cn)

Tel: +86-13699130626

## Abstract

Although there are many reports on the removal of NO<sub>x</sub> from vehicle and power plant emissions, little effort has been devoted to the removal of NO<sub>x</sub> from cracker flue gases. Here we report a systematic investigation on the design of highly efficient NO<sub>x</sub> storage-reduction (NSR) catalysts using highly dispersed aqueous miscible organic-layered double hydroxides (AMO-LDHs) derived mixed oxides (LDOs) for NO<sub>x</sub> emission control from naphtha cracker flue gases. For a series of binary M<sup>2+</sup>Al<sup>3+</sup> LDOs, the influence of six divalent cations (Ca, Zn, Cu, Ni, Co, and Mg) on the NO<sub>x</sub> adsorption capacity, NO oxidation property, and the thermal stability of adsorbed NO<sub>x</sub> was systematically investigated. The optimal NO<sub>x</sub> storage temperature range for each binary LDO was also determined. Based on the fundamental findings of binary LDOs, a ternary LDH CoMgAl-CO<sub>3</sub> derived LDO CoMgAlO<sub>x</sub> with a significantly improved NO<sub>x</sub> storage capacity was designed. By tuning the Co/Mg ratio, the NO<sub>x</sub> storage capacity was greatly improved from 0.14 mmol/g for Mg<sub>3</sub>Al<sub>1</sub>O<sub>x</sub> to 0.50 mmol/g for Co<sub>1</sub>Mg<sub>2</sub>Al<sub>1</sub>O<sub>x</sub> at 300 °C. By further doping Pt and K<sub>2</sub>CO<sub>3</sub>, a new NSR catalyst composed of 1 wt% Pt/15 wt% K<sub>2</sub>CO<sub>3</sub>/Co<sub>1</sub>Mg<sub>2</sub>Al<sub>1</sub>O<sub>x</sub> was obtained, which exhibited a very high NO<sub>x</sub> storage capacity of 1.2 mmol/g. Finally, the NSR cycling performance, and the CO<sub>2</sub>, SO<sub>2</sub> and H<sub>2</sub>O resistance of this catalyst were also investigated. Thanks for its superior NO<sub>x</sub> storage capacity, NSR cycling performance, and CO<sub>2</sub>, SO<sub>2</sub> and H<sub>2</sub>O resistance, this new NSR catalyst showed great potential for the NO<sub>x</sub> control from cracker flue gases.

**Keywords:** layered double hydroxides, layered double oxide, NO<sub>x</sub> abatement, cracker flue gas, mixed metal oxides, AMOST method

## 1. Introduction

As a result of increasingly stringent emission regulations, the abatement of  $\text{NO}_x$  from flue gases of naphtha crackers has become a critical issue. However, so far there are only very few studies on the removal of  $\text{NO}_x$  from naphtha crackers flue gases, whose  $\text{NO}_x$  concentration is normally quite low (50–100 ppm). In addition to  $\text{NO}_x$ , the naphtha crackers flue gases also contain many other components including  $\text{CO}_2$  (7.5–9.5%),  $\text{H}_2\text{O}$  (14–17%),  $\text{O}_2$  (3–5%),  $\text{SO}_2$  (0.1–1 ppm).[1] Considering the fact that the flow rate of flue gases is very high and the concentration of  $\text{NO}_x$  is low, the  $\text{NO}_x$  storage and reduction (NSR) technology is proposed to be promising.[2, 3]

NSR catalysts have been well studied for the abatement of  $\text{NO}_x$  from vehicle emissions. They store  $\text{NO}_x$  as nitrates (or nitrite) under lean conditions and allow nitrate (or nitrite) decomposition and  $\text{NO}_x$  reduction during short rich conditions.[4] Typical NSR catalysts consist of a high surface area support (e.g.  $\gamma\text{-Al}_2\text{O}_3$ ,  $\text{TiO}_2$ ,  $\text{ZrO}_2$ , or  $\text{TiO}_2\text{-ZrO}_2$ ), a  $\text{NO}_x$  storage component (alkaline or earth alkaline metal oxide, e.g.,  $\text{BaO}$ ,  $\text{K}_2\text{O}$ ,  $\text{CaO}$ , or  $\text{MgO}$ ), and a noble metal (e.g. Pt or Rh).[5-12] The most widely studied and prototypical NSR catalyst is Pt-BaO/ $\gamma\text{-Al}_2\text{O}_3$ , as developed by Toyota.[4, 7, 13, 14] Although much effort has been devoted to the Pt-BaO/ $\gamma\text{-Al}_2\text{O}_3$  catalyst system, catalyst deactivations especially thermal deterioration and sulfur poisoning have hindered its commercial application in automobiles.[4] [7, 15] Furthermore, substantial effort has been made to further improve the performance of Pt-BaO/ $\text{Al}_2\text{O}_3$  NSR catalyst by introducing other components such as e.g. Fe, Ce, Cu, and Ni.[16, 17] However, the search for alternative catalysts has also drawn much attention,[17-20] for example, perovskite-type,[21-23] zeolite-type,[17] and potassium dititanate-type, etc.[11, 12, 24] Recently, well-dispersed mixed metal oxides derived from layered double hydroxides (LDHs) have received considerable attention as alternative NSR

catalysts.[20, 25]

LDHs are a class of ionic lamellar compounds made up of positively charged brucite-like layers, with an interlayer region containing charge compensating anions and solvation molecules. LDHs have been widely used as ion exchangers, adsorbents, base catalysts, and precursors of well-mixed oxides for various catalytic applications.[26, 27] The most widely studied LDHs contain both divalent and trivalent metal cations, and the generic formula for these LDHs can be written as  $[M^{2+}_{1-x}M^{3+}_x(OH)_2][A^{n-}]_{x/n} \cdot zH_2O$ , where  $M^{2+}$  is divalent cation such as  $Mg^{2+}$ ,  $Zn^{2+}$ ,  $Co^{2+}$ ,  $Ca^{2+}$ ,  $Cu^{2+}$  or  $Ni^{2+}$ , and  $M^{3+}$  is trivalent cation such as  $Al^{3+}$ ,  $Ga^{3+}$ ,  $Fe^{3+}$ , or  $Mn^{3+}$ .  $A^{n-}$  is a non-framework charge compensating inorganic, bioorganic or organic anion such as  $CO_3^{2-}$ ,  $Cl^-$ ,  $SO_4^{2-}$ , or  $RCO_2^-$ , and  $x$  is normally in the range 0.2–0.4.[26] One issue for the LDHs derived functional materials is the severe aggregation during preparation. Recently, we developed a simple and facile method to meet this challenge, which we have named the aqueous miscible organic solvent treatment (AMOST) method.[28, 29] In this method, an aqueous miscible organic solvent is used in a post treatment step on the wet LDH slurry that may be synthesised by any conventional method. This relatively simple and scalable procedure very efficiently increases the specific surface area (SSA) and pore volume and improves the dispersion capacity of the LDH particles in non-polar hydrocarbon solvents. LDHs obtained using this method have been named AMO-LDHs. Calcination on an AMO-LDH between 300–550 °C produces high surface mixed metal oxides that we call AMO-LDOs. The chemical versatility of the metal composition within LDHs and our recent ability to make high surface area materials makes it a very flexible platform to prepare and study a range of high surface area mixed metal oxides as potential NSR catalysts.[30] In this paper, all LDHs and LDOs were obtained using this new AMOST synthesis

method.

In order to utilise the NSR technology to remove NO<sub>x</sub> from naphtha cracker flue gases, selecting an efficient NO<sub>x</sub> trapping material is of critical importance. In this contribution, we have carried out a comprehensive study of the divalent cation dependent NO<sub>x</sub> storage capacity of AMO-LDOs formed on calcination of the corresponding highly dispersed AMO-LDHs. The influence of divalent cations on the NO<sub>x</sub> adsorption property, NO oxidation, thermal stability of adsorbed NO<sub>x</sub>, and CO<sub>2</sub> and SO<sub>2</sub> resistance of six potential binary AMO-LDOs including Mg<sub>3</sub>Al<sub>1</sub>O<sub>x</sub>, Co<sub>3</sub>Al<sub>1</sub>O<sub>x</sub>, Ni<sub>3</sub>Al<sub>1</sub>O<sub>x</sub>, Cu<sub>3</sub>Al<sub>1</sub>O<sub>x</sub>, Zn<sub>3</sub>Al<sub>1</sub>O<sub>x</sub>, Ca<sub>2</sub>Al<sub>1</sub>O<sub>x</sub> were systematically investigated. Based on these results, a promising ternary CoMgAl-CO<sub>3</sub> LDH derived mixed oxide CoMgAlO<sub>x</sub> was designed with significantly improved NO<sub>x</sub> storage capacity. Finally, a novel NSR catalyst Pt-K<sub>2</sub>CO<sub>3</sub>/CoMgAlO<sub>x</sub> was developed by doping Pt and a second NO<sub>x</sub> storage compound K<sub>2</sub>CO<sub>3</sub>. [31, 32] The influences of Co/Mg ratio, loadings of Pt and K<sub>2</sub>CO<sub>3</sub>, lean-rich cycling performance, and presence of CO<sub>2</sub>, SO<sub>2</sub> and H<sub>2</sub>O on the NO<sub>x</sub> storage performance of Pt-K<sub>2</sub>CO<sub>3</sub>/CoMgAlO<sub>x</sub> were also studied. Due to its high NO<sub>x</sub> storage capacity and excellent lean-rich cycling performance, this novel NSR catalyst is very promising for the abatement of NO<sub>x</sub>.

## 2. Experimental

### 2.1. Sample preparation

**Synthesis of binary LDHs.** [M<sub>3</sub>Al(OH)<sub>8</sub>](CO<sub>3</sub>)<sub>0.5</sub>·xH<sub>2</sub>O LDHs (M = Mg<sup>2+</sup>, Zn<sup>2+</sup>, Co<sup>2+</sup>, Cu<sup>2+</sup> or Ni<sup>2+</sup>) were synthesised via a conventional coprecipitation method, followed by an AMOST treatment with acetone.[29] In brief, a salt solution (100 mL) containing a mixture of 0.075 mol M(NO<sub>3</sub>)<sub>2</sub>·6H<sub>2</sub>O (M = Mg<sup>2+</sup>, Zn<sup>2+</sup>, Cu<sup>2+</sup>, Co<sup>2+</sup> and Ni<sup>2+</sup>) and 0.025 mol Al(NO<sub>3</sub>)<sub>3</sub>·9H<sub>2</sub>O was added drop-wise to a basic solution (100 mL)

containing 0.05 mol  $\text{Na}_2\text{CO}_3$ . While for  $\text{Ca}_2\text{Al}_1\text{-NO}_3$  LDH,  $\text{Ca}(\text{NO}_3)_2$  was used and the above used  $\text{Na}_2\text{CO}_3$  was replaced by  $\text{NaNO}_3$ . The pH value of the precipitation solution was kept constant at  $\text{pH} = 10$  by the addition of a solution containing 4 M  $\text{NaOH}$ . The resulting mixture solution was aged at room temperature for 12 h with continuous stirring. The samples were filtered and washed with deionised water until  $\text{pH} = 7$ . The obtained LDH slurry was re-dispersed in acetone, stirred for 2 h, and washed with acetone thoroughly. The obtained samples are dried at  $60\text{ }^\circ\text{C}$  in an oven.

**Synthesis of CoMgAl- $\text{CO}_3$  ternary LDHs.** The CoMgAl- $\text{CO}_3$  LDHs with different Co/Mg ratios were synthesized via the recently developed AMOST method as well.[29] In brief, a salt solution (100 mL) containing a mixture of 0.075 mmol  $\text{Co}(\text{NO}_3)_2 \cdot 6\text{H}_2\text{O}$  and  $\text{Mg}(\text{NO}_3)_2 \cdot 6\text{H}_2\text{O}$ , and 0.025 mol  $\text{Al}(\text{NO}_3)_3 \cdot 9\text{H}_2\text{O}$  were added drop-wise to a basic solution (100 mL) containing 0.05 mol  $\text{Na}_2\text{CO}_3$ . The ratio of Co/Mg can be precisely controlled by selecting proper amount of  $\text{Co}(\text{NO}_3)_2 \cdot 6\text{H}_2\text{O}$  and  $\text{Mg}(\text{NO}_3)_2 \cdot 6\text{H}_2\text{O}$  precursors. The pH value of the precipitation solution was kept constant at 10 by addition of a solution containing 4 M  $\text{NaOH}$ . The resulting mixture solution was aged at room temperature for 12 h with continuous stirring. The aged mixture was filtered and washed with deionized water until  $\text{pH} = 7$ . Then the sample was re-dispersed in acetone solution again. After stirring for about 1–2 h, the sample was filtered and washed with acetone thoroughly. The final LDH product was dried at  $60\text{ }^\circ\text{C}$ .

**Synthesis of Pt/CoMgAlO<sub>x</sub>.** Pt/CoMgAlO<sub>x</sub> was prepared via an impregnation method. LDH was first thermally pretreated at  $400\text{ }^\circ\text{C}$  for 5 h in air. Then the obtained LDO was dispersed in 10 mL of  $\text{H}_2\text{PtCl}_6$  ethanol solution, followed by drying in oven overnight. These steps were repeated to control the Pt loading to be 1, 2, and 4 wt%, respectively. Finally, the samples were further calcined at  $400\text{ }^\circ\text{C}$  for 5 h in air to

obtain the Pt/CoMgAlO<sub>x</sub>.

**Synthesis of K<sub>2</sub>CO<sub>3</sub>/CoMgAlO<sub>x</sub>.** K<sub>2</sub>CO<sub>3</sub>/CoMgAlO<sub>x</sub> was prepared via an incipient wetness impregnation method. LDH was first pretreated at 400 °C for 5 h. Then K<sub>2</sub>CO<sub>3</sub> ethylene glycol solution was added drop-wise to the calcined LDH until it appeared wet, followed by drying in an oven for overnight. These steps were repeated to control the K<sub>2</sub>CO<sub>3</sub> loading to be 5, 10, 15, 20, and 25 wt%, respectively. Finally, the samples were further calcined at 400 °C in air for 5 h to obtain the K<sub>2</sub>CO<sub>3</sub>/CoMgAlO<sub>x</sub>.

**Synthesis of Pt-K<sub>2</sub>CO<sub>3</sub>/CoMgAlO<sub>x</sub>.** After obtaining the K<sub>2</sub>CO<sub>3</sub>/CoMgAlO<sub>x</sub>, it was then dispersed in 10 mL of H<sub>2</sub>PtCl<sub>6</sub> ethanol solution, followed by drying in oven overnight. Finally, the samples were further calcined at 400 °C in air for 5 h to obtain the Pt-K<sub>2</sub>CO<sub>3</sub>/CoMgAlO<sub>x</sub>.

## 2.2. Catalyst characterization

XRD patterns of samples were measured on a Shimadzu XRD-7000 instrument in reflection mode with Cu K $\alpha$  radiation. The accelerating voltage was set at 40 kV with 30 mA current ( $\lambda = 1.542 \text{ \AA}$ ) at 5 degree per min from 5 to 70°. The BET (Brunauer, Emmet, and Teller) specific surface areas were measured from the N<sub>2</sub> adsorption and desorption isotherms at 77 K collected from a Builder SSA-700 surface area and pore size analyzer. The morphologies of samples were characterized using field emission scanning electron microscope (FE-SEM, SU-8020). Before observation, the samples were sputter coated with a thin platinum layer to prevent charging and to improve the image quality. High resolution transmission electron microscopy (HR-TEM) was performed on JEM-2100 microscope (JEOL, Japan) with an accelerating voltage of 200 kV.

## 2.3. Measurement of NO<sub>x</sub> storage capacity

All catalytic tests including isothermal NO<sub>x</sub> adsorption, lean-rich cycling, and temperature programmed desorption (TPD) were performed in a fixed-bed quartz flow reactor at atmosphere pressure. For each test, 0.05–0.2 g catalyst was placed in the reactor. For monitoring the feed compositions and reaction products, a NO<sub>x</sub> analyzer (NO-NO<sub>2</sub>-NO<sub>x</sub> analyzer, Model 42i-HL, Thermo, US) and an on-line quadrupole mass spectrometer (QGA, Hidden, UK) were equipped. For the isothermal NO<sub>x</sub> adsorption tests, a gas mixture containing 100 ppm NO<sub>x</sub>, 10% O<sub>2</sub>, and the balance Ar with a total flow rate of 300 mL/min was used. For the lean-rich cycling tests, the 15 min lean and 3 min rich atmospheres were alternatively switched. The gas mixture for lean condition contains 100 ppm NO, 10% O<sub>2</sub>, and the balance Ar (300 mL/min), and the gas mixture for rich condition contains 100 ppm NO, 3.5% H<sub>2</sub>, and the balance Ar (300 mL/min). For testing the influence of water vapor, 5% H<sub>2</sub>O will be added to the input gases. For NO<sub>x</sub>-TPD tests, after adsorbing NO<sub>x</sub> at 300 °C for 1 h, the catalyst was cooled down to room temperature without any flow gas. At room temperature, any weakly adsorbed species were removed by purging pure Ar at 300 mL/min. Then the furnace was heated from room temperature to 600 °C with a ramp rate of 2 °C/min in 300 mL/min Ar.

### **3. Results and discussion**

#### **3.1. NO<sub>x</sub> storage performance of binary LDOs**

In order to have a comprehensive understanding of the influence of divalent cation on the NO<sub>x</sub> storage performance of LDOs formed on calcination of the corresponding highly dispersed AMO-LDHs, six potential binary LDHs including Ca<sub>2</sub>Al<sub>1</sub>-NO<sub>3</sub>, Zn<sub>3</sub>Al<sub>1</sub>-CO<sub>3</sub>, Cu<sub>3</sub>Al<sub>1</sub>-CO<sub>3</sub>, Mg<sub>3</sub>Al<sub>1</sub>-CO<sub>3</sub>, Co<sub>3</sub>Al<sub>1</sub>-CO<sub>3</sub>, and Ni<sub>3</sub>Al<sub>1</sub>-CO<sub>3</sub> were prepared and thoroughly investigated for NO<sub>x</sub> adsorption. All obtained samples were initially

characterised using XRD analysis, as shown in Fig. S1. It is clear that all samples have formed a typical layered double hydroxide structure. The characteristic reflections of  $M_3Al_1CO_3$  ( $M = Mg, Zn, Co, Cu$  or  $Ni$ ) LDHs at  $2\theta = 11.29^\circ, 22.73^\circ, 34.48^\circ, 39.18^\circ, 46.24^\circ, 60.36^\circ$ , and  $61.20^\circ$  were clearly observed, which can be indexed as of (003), (006), (009), (015), (018), (110), and (113) Bragg reflections respectively. The corresponding PDF card number for  $Mg_3Al_1CO_3$ ,  $Co_3Al_1CO_3$ ,  $Cu_3Al_1CO_3$ , and  $Ni_3Al_1CO_3$  LDHs is JCPDS 35-0965, 51-0045, 37-0630, and 48-0594, respectively.[33] While for  $Ca_2Al_1NO_3$  LDH, the first three reflections can be indexed to (002), (004), and (006) Bragg reflections, respectively.[34] The morphologies of the as prepared various binary LDHs were observed using FE-SEM analysis. As shown in Fig. S2,  $Ca_2Al_1NO_3$  and  $Cu_3Al_1CO_3$  LDHs exhibited “plate-like” particles, while  $Mg_3Al_1CO_3$  LDHs showed a spheroidal “sand rose” morphology. Samples of  $Zn_3Al_1CO_3$ ,  $Ni_3Al_1CO_3$ , and  $Co_3Al_1CO_3$  LDHs are aggregates consisting of irregular nanoparticles with an average size of ca. 30–50 nm. The SSA, pore volume, and pore size of LDOs obtained by thermal calcination of the corresponding LDHs were measured using BET method, as shown in Table S1. The  $Mg_3Al_1O_x$  LDO formed by calcination of  $Mg_3Al_1CO_3$  LDH showed the highest BET SSA of  $329.6\text{ m}^2/\text{g}$  and pore volume of  $1.5\text{ cm}^3/\text{g}$ . While for  $Cu_3Al_1O_x$ , the BET SSA and pore volume were low, which was  $93.0\text{ m}^2/\text{g}$  and  $0.55\text{ cm}^3/\text{g}$ , respectively. For  $Co_3Al_1O_x$  and  $Ni_3Al_1O_x$ , the SSA was 122.5 and  $202.0\text{ m}^2/\text{g}$ , respectively.

The influence of divalent cations ( $Mg, Ca, Zn, Co, Ni$ , and  $Cu$ ) in LDOs on their  $NO_x$  adsorption capacity in the temperature range of 90–400 °C was systematically investigated using isothermal  $NO_x$  adsorption. Both  $Ca_2Al_1O_x$  and  $Zn_3Al_1O_x$  possess negligible  $NO_x$  adsorption in the temperature range 90–400 °C (Fig. S3). Fig. 1(a) and (b) show the  $NO_x$  adsorption capacity of  $Ni_3Al_1O_x$  and  $Cu_3Al_1O_x$  as a function of

temperature. For both  $\text{Ni}_3\text{Al}_1\text{O}_x$  and  $\text{Cu}_3\text{Al}_1\text{O}_x$  there is a general trend that their  $\text{NO}_x$  adsorption capacity generally increased with the decrease in adsorption temperature. For  $\text{Ni}_3\text{Al}_1\text{O}_x$ , its  $\text{NO}_x$  adsorption capacity was 0.1 mmol/g at 300 °C, which increased to 0.23 mmol/g at 250 °C, and kept almost unchanged in the temperature range of 120–250 °C. A similar trend was observed with  $\text{Cu}_3\text{Al}_1\text{O}_x$ . At 180–250 °C, its  $\text{NO}_x$  storage capacity was very low, only 0.03 mmol/g, but its  $\text{NO}_x$  adsorption capacity was increased to 0.09 mmol/g at 150 °C, and kept almost unchanged (0.14 mmol/g) between 90–120 °C.

The temperature dependent  $\text{NO}_x$  adsorption performance for  $\text{Co}_3\text{Al}_1\text{O}_x$  and  $\text{Mg}_3\text{Al}_1\text{O}_x$  showed different trends. For  $\text{Co}_3\text{Al}_1\text{O}_x$ , its  $\text{NO}_x$  storage capacity first increased with the increase in adsorption temperature from 90 to 150 °C, and then decreased with the adsorption temperature in the range 180–300 °C. The optimal  $\text{NO}_x$  adsorption temperature for  $\text{Co}_3\text{Al}_1\text{O}_x$  is in the range 150–180 °C, at which the highest adsorption capacity was 0.21 mmol/g. While for  $\text{Mg}_3\text{Al}_1\text{O}_x$ , its  $\text{NO}_x$  storage capacity gradually increased with the increase in adsorption temperature from 90–400 °C, and the highest  $\text{NO}_x$  storage capacity of 0.26 mmol/g was obtained at 400 °C. These data suggested that  $\text{Co}_3\text{Al}_1\text{O}_x$  is a good intermediate-temperature (150–180 °C)  $\text{NO}_x$  trapping material, and  $\text{Mg}_3\text{Al}_1\text{O}_x$  a good high-temperature (400 °C)  $\text{NO}_x$  trapping material. Lamb et al.[35] have reported that a conventionally prepared  $\text{Mg}_3\text{Al}_1\text{O}_x$  showed a  $\text{NO}_x$  storage capacity of 0.019 mmol/g. In contrast, the  $\text{Mg}_3\text{Al}_1\text{O}_x$  prepared from AMO-LDH precursor shows an almost 14 times higher  $\text{NO}_x$  storage capacity of 0.26 mmol/g. Such high  $\text{NO}_x$  storage capacity of  $\text{Mg}_3\text{Al}_1\text{O}_x$  from AMO-LDH precursor can be attributed to its much higher specific surface area than the conventional sample as we discovered previously.[29, 30] Except for the physical properties, the surface basic sites of  $\text{Mg}_3\text{Al}_1\text{O}_x$  from AMO-LDH precursor were also

compared with the conventional water washed sample using CO<sub>2</sub>-TPD analysis, as shown in Fig. S4. It can be clearly seen that our Mg<sub>3</sub>AlO<sub>x</sub> sample from AMOST method adsorbed much more CO<sub>2</sub> than the conventional one, suggesting that it possesses much more surface basic sites.

The optimal NO<sub>x</sub> storage temperature range and their corresponding NO<sub>x</sub> storage capacity of Zn<sub>3</sub>Al<sub>1</sub>O<sub>x</sub>, Cu<sub>3</sub>Al<sub>1</sub>O<sub>x</sub>, Ni<sub>3</sub>Al<sub>1</sub>O<sub>x</sub>, Ca<sub>2</sub>Al<sub>1</sub>O<sub>x</sub>, Co<sub>3</sub>Al<sub>1</sub>O<sub>x</sub>, and Mg<sub>3</sub>Al<sub>1</sub>O<sub>x</sub> LDOs were summarised in Fig. 2. The data clearly shows that the divalent cation plays a significant role on their NO<sub>x</sub> storage behaviour. For Zn<sub>3</sub>Al<sub>1</sub>O<sub>x</sub>, Cu<sub>3</sub>Al<sub>1</sub>O<sub>x</sub>, and Ca<sub>2</sub>Al<sub>1</sub>O<sub>x</sub>, their optimal NO<sub>x</sub> adsorption temperatures are lower, in the range of 90–150 °C. And comparing to other LDOs, their NO<sub>x</sub> storage capacity were much worse, which was less than 0.14 mmol/g. Ni<sub>3</sub>Al<sub>1</sub>O<sub>x</sub> showed relatively good NO<sub>x</sub> adsorption performance over a wide temperature range (120–250 °C), with a constant capacity of 0.23 mmol/g. Co<sub>3</sub>Al<sub>1</sub>O<sub>x</sub> showed good intermediate-temperature NO<sub>x</sub> adsorption in the range of 150–180 °C, and Mg<sub>3</sub>Al<sub>1</sub>O<sub>x</sub> showed good high-temperature NO<sub>x</sub> adsorption at 400 °C. Based on literature reports, it was speculated that the difference in NO<sub>x</sub> adsorption characteristics between different LDOs should be related to the NO oxidation activity and the stability of adsorbed NO<sub>x</sub> on various LDOs. In order to prove this assumption, additional experiments were carried out.

As it is well known that the NO<sub>x</sub> adsorption is actually a two-step process, which includes the initial NO oxidation to NO<sub>2</sub> and the subsequent NO<sub>2</sub> adsorption as nitrate/nitrite. Thus, in order to prove whether the NO oxidation to NO<sub>2</sub> is a limiting step, Mg<sub>3</sub>Al<sub>1</sub>O<sub>x</sub> and Co<sub>3</sub>Al<sub>1</sub>O<sub>x</sub> LDOs were doped with Ag in order to promote the NO oxidation to NO<sub>2</sub>. Fig. S5 shows that the Ag has good NO oxidation property to NO<sub>2</sub>. The NO<sub>x</sub> storage capacities of Ag/Mg<sub>3</sub>Al<sub>1</sub>O<sub>x</sub> and Ag/Co<sub>3</sub>Al<sub>1</sub>O<sub>x</sub> were then evaluated with NO + O<sub>2</sub> at 90–300 °C. Fig. S6(a) shows the effect of Ag loading on Mg<sub>3</sub>Al<sub>1</sub>O<sub>x</sub>

at 90 °C. The data indicates a 3 fold increase in the NO<sub>x</sub> storage capacity from 0.10 to 0.32 mmol/g at an optimal Ag loading of 4 wt%. Fig. S6(b) shows the influence of adsorption temperature (90–300 °C) on the NO<sub>x</sub> storage capacity of 4 wt% Ag/Mg<sub>3</sub>Al<sub>1</sub>O<sub>x</sub>, which suggests that significant promoting effect was achieved in the whole temperature range. The NO<sub>x</sub> storage capacities at 90, 150, and 300 °C were all experienced a significant increase from 0.1, 0.13, 0.14 mmol/g to 0.32, 0.32, and 0.38 mmol/g, respectively. While for Co<sub>3</sub>Al<sub>1</sub>O<sub>x</sub>, Ag doping only showed a negligible effect on its NO<sub>x</sub> storage capacity (Fig. S6(c) and (d)). This probably because Co<sub>3</sub>Al<sub>1</sub>O<sub>x</sub> already has relatively good NO oxidation and thus it could not be further promoted by Ag doping. While for Mg<sub>3</sub>Al<sub>1</sub>O<sub>x</sub>, since its NO oxidation activity is poor, it could be significantly promoted by Ag doping. In order to provide a direct evidence that the NO oxidation to NO<sub>2</sub> is a key step, the NO<sub>x</sub> storage capacities of LDOs in the presence of NO<sub>2</sub> rather than NO+O<sub>2</sub> were also tested, as shown in Fig. S7. The NO<sub>x</sub> storage capacities were increased by ca. 0.11–0.15 mmol/g for Co<sub>3</sub>AlO<sub>x</sub>, Cu<sub>3</sub>AlO<sub>x</sub>, and Mg<sub>3</sub>AlO<sub>x</sub>, which further confirmed that the NO oxidation to NO<sub>2</sub> step is crucial. The NO<sub>x</sub> storage and NO oxidation tests demonstrated that different divalent cations have different NO oxidation activity as well as different NO<sub>x</sub> storage capacity.

For the NO<sub>x</sub> trapping materials, not only the NO<sub>x</sub> storage capacity but also the thermal stability of adsorbed NO<sub>x</sub> is important. Thus, the thermal stability of adsorbed NO<sub>x</sub> on four representative binary LDOs including Cu<sub>3</sub>Al<sub>1</sub>O<sub>x</sub>, Co<sub>3</sub>Al<sub>1</sub>O<sub>x</sub>, Ni<sub>3</sub>Al<sub>1</sub>O<sub>x</sub>, and Mg<sub>3</sub>Al<sub>1</sub>O<sub>x</sub> were evaluated using a TPD method, as shown in Fig. S8. After adsorbing NO<sub>x</sub> at 150 °C for 1 h, the samples were cooled to room temperature. Then the samples were heated from room temperature to 600 °C with a ramp rate of 2 °C/min, and the concentration of desorbed NO<sub>x</sub> was monitored using a NO<sub>x</sub> analyzer. The peak NO<sub>x</sub> desorption temperature of each LDO was summarised in Fig.

S9. The thermal desorption temperature for NO<sub>x</sub> follows the order Mg<sub>3</sub>Al<sub>1</sub>O<sub>x</sub> > Ni<sub>3</sub>Al<sub>1</sub>O<sub>x</sub> > Cu<sub>3</sub>Al<sub>1</sub>O<sub>x</sub> > Co<sub>3</sub>Al<sub>1</sub>O<sub>x</sub>, with a peak desorption temperature of 500, 390, 320, and 290 °C, respectively. This NO<sub>x</sub>-TPD data demonstrated that the divalent cations have great effect on the thermal stability of adsorbed NO<sub>x</sub>.

It is well known that LDOs have relatively good CO<sub>2</sub> adsorption capacity, particularly at 200–400 °C.[36-38] The flue gases used in this work contain 9% CO<sub>2</sub>, which may compete the adsorption sites with NO<sub>x</sub>. Thus the influence of CO<sub>2</sub> on the NO<sub>x</sub> storage capacity of various LDOs including Mg<sub>3</sub>Al<sub>1</sub>O<sub>x</sub>, Cu<sub>3</sub>Al<sub>1</sub>O<sub>x</sub>, Ni<sub>3</sub>Al<sub>1</sub>O<sub>x</sub>, and Co<sub>3</sub>Al<sub>1</sub>O<sub>x</sub> were investigated as well. Fig. 3 shows that most LDOs were less effected by CO<sub>2</sub> at low temperatures (90–150 °C), except for Cu<sub>3</sub>Al<sub>1</sub>O<sub>x</sub>. At higher temperatures (250–400 °C), Mg<sub>3</sub>Al<sub>1</sub>O<sub>x</sub> and Ni<sub>3</sub>Al<sub>1</sub>O<sub>x</sub> were significantly influenced, while Cu<sub>3</sub>Al<sub>1</sub>O<sub>x</sub> and Co<sub>3</sub>Al<sub>1</sub>O<sub>x</sub> were less influenced. The NO<sub>x</sub> adsorption tests in the presence of 9% CO<sub>2</sub> indicated that different binary LDOs have different CO<sub>2</sub> resistance properties.

The above results revealed that different LDOs have different NO<sub>x</sub> storage performance, which can be attributed to their difference in NO<sub>x</sub> adsorption capacity, NO oxidation property, and thermal stability of adsorbed NO<sub>x</sub>. For instance, MgAlO<sub>x</sub> is good for NO<sub>x</sub> storage, but poor for NO oxidation. CoAlO<sub>x</sub> is good for NO oxidation, but poor for NO<sub>x</sub> storage. They also have different CO<sub>2</sub> resistant property. Based on these results, we expect that by combining the good NO oxidation property of Co and good NO<sub>x</sub> adsorption property of Mg, a better NO<sub>x</sub> adsorbent could be developed. Thus, in the following section, we then systematically investigated the NO<sub>x</sub> storage performance of a ternary LDO CoMgAlO<sub>x</sub>.

### **3.2. NO<sub>x</sub> storage performance of ternary CoMgAlO<sub>x</sub> LDOs**

From the above investigation on the influence of divalent cations in the mixed metal oxide, we have proved that both CoAlO<sub>x</sub> and MgAlO<sub>x</sub> have a relatively higher NO<sub>x</sub>

storage capacity than other binary LDOs. For  $\text{MgAlO}_x$ , Mg phase is good for  $\text{NO}_x$  storage but poor for NO oxidation. While for  $\text{CoAlO}_x$ , the Co phase is good for NO oxidation, but relatively poor for  $\text{NO}_x$  storage. Therefore, we proceeded to try and combine the features of both of  $\text{Co}^{2+}$  and  $\text{Mg}^{2+}$  by synthesising ternary  $\text{CoMgAl-CO}_3$  LDH. Five  $\text{CoMgAl-CO}_3$  LDHs with different Co/Mg atomic ratios (0.25, 0.5, 1, 1.5 and 2, respectively) were synthesized using AMOST method.

The obtained samples were first characterized using XRD analysis, as shown in Fig. 4(a). It is clear that all the five ternary LDHs have formed a typical layered double hydroxide structure. The characteristic Bragg reflections of  $\text{Co}_x\text{Mg}_{3-x}\text{Al}_1\text{-CO}_3$  LDH were clearly observed at  $2\theta = 11.29^\circ, 22.73^\circ, 34.48^\circ, 39.18^\circ, 46.24^\circ, 60.36^\circ$ , and  $61.20^\circ$ , which can be attributed to reflections of (003), (006), (009), (015), (018), (110), and (113) planes, respectively. Fig. 4(b) shows the XRD patterns of LDOs obtained by calcination of  $\text{Co}_x\text{Mg}_{3-x}\text{Al}_1\text{-CO}_3$  LDHs at  $400^\circ\text{C}$ . All LDHs lost their layered structure and turned into mixed oxides. When the Co loading was low, the major phase was periclase MgO. However, with the increase in Co loading, the major phase gradually changed to Co related phases. The Co-related phases were observed at  $22.18^\circ, 36.68^\circ, 43.18^\circ, 59.35^\circ$ , and  $65.78^\circ$ , which can be attributed to  $\text{Co}_3\text{O}_4$  and/or  $\text{CoAl}_2\text{O}_4$ . The morphologies of synthesized various  $\text{Co}_x\text{Mg}_{3-x}\text{Al}_1\text{-CO}_3$  LDHs were observed using FE-SEM analysis, as shown in Fig. S10. When the Co/Mg ratio was low ( $< 1$ ), the samples formed typical spheroidal “sand rose” morphology. This is because  $\text{Mg}_3\text{Al}_1\text{-CO}_3$  tends to form “sand rose” morphology when the synthesis pH was controlled at 10.[39] However, with the increase in Co/Mg ratio, the morphology gradually changed from “sand rose” to nanoplate-like, which is because  $\text{Co}_3\text{Al}_1\text{-CO}_3$  tends to form plate-like morphology.

For comparison, the isothermal  $\text{NO}_x$  storage on  $\text{Co}_x\text{Mg}_{3-x}\text{Al}_1\text{-CO}_3$  LDHs with

different Co/Mg atomic ratios at different adsorption temperatures was carried out. As summarized in the Fig. 5, the catalysts derived from  $\text{Co}_x\text{Mg}_{3-x}\text{Al}_1\text{-CO}_3$  LDHs have much improved  $\text{NO}_x$  storage capacities than  $\text{Mg}_3\text{Al}_1\text{O}_x$ . At low temperature (90 °C), the  $\text{NO}_x$  storage capacity increased with the increase in Co content. The sample  $\text{Co}_{1.5}\text{Mg}_{1.5}\text{Al}_1\text{-CO}_3$  showed the highest  $\text{NO}_x$  storage capacity of 0.47 mmol/g. When the adsorption temperature was increased to 150 °C, the  $\text{NO}_x$  adsorption capacity of all these  $\text{Co}_x\text{Mg}_{3-x}\text{Al}_1\text{O}_y$  catalysts showed a decreasing trend except for  $\text{Co}_{0.5}\text{Mg}_{2.5}\text{Al}_1\text{O}_x$ , which may due to the oxidation activity of NO decreased with the increase in adsorption temperature. However, the  $\text{NO}_x$  storage performance in the high temperature range (250–300 °C) was quite different,  $\text{Co}_{0.5}\text{Mg}_{2.5}\text{Al}_1\text{O}_x$  and  $\text{Co}_1\text{Mg}_2\text{Al}_1\text{O}_x$  exhibited a high  $\text{NO}_x$  storage capacity of 0.49 and 0.50 mmol/g, respectively. In this work, we prefer to have a catalyst that has better NO oxidation activity, so that  $\text{Co}_1\text{Mg}_2\text{Al}_1\text{O}_x$  was selected for further investigations.

### 3.3. $\text{NO}_x$ storage and lean–rich cycling performance of Pt- $\text{K}_2\text{CO}_3/\text{CoMgAlO}_x$

It was suggested that doping LDOs with Pt and  $\text{K}_2\text{CO}_3$  can enhance their  $\text{NO}_x$  storage capacity. Thus, the  $\text{NO}_x$  storage performance of Pt and  $\text{K}_2\text{CO}_3$  doped  $\text{Co}_1\text{Mg}_2\text{Al}_1\text{O}_x$  catalysts were studied. The influence of the Pt loading (1–4 wt%) and  $\text{K}_2\text{CO}_3$  content (5–25 wt%) were systematically studied. The phase structures of 1 wt% Pt/ $\text{Co}_1\text{Mg}_2\text{Al}_1\text{O}_x$  and 1 wt% Pt-15 wt%  $\text{K}_2\text{CO}_3/\text{Co}_1\text{Mg}_2\text{Al}_1\text{O}_x$  were first characterized using XRD analysis (Fig. 6(a)). All the diffraction peaks in the patterns are attributed to mixed oxides, no diffraction peaks corresponding to Pt- or K-related species appear, which indicates that both Pt and  $\text{K}_2\text{CO}_3$  species should be present in the amorphous or in highly dispersed state on the support surface. Many works reported a similar phenomenon that the Pt- and K-containing species are hardly recognized by XRD analysis.[40, 41] Thus, it is deduced that the  $\text{K}_2\text{CO}_3$  phase probably exists in

amorphous state and that the Pt concentration may be below the XRD detection limit.[41]

The morphologies of  $\text{Co}_1\text{Mg}_2\text{Al}_1\text{-CO}_3$  LDH,  $\text{Co}_1\text{Mg}_2\text{Al}_1\text{O}_x$  LDO, 15 wt%  $\text{K}_2\text{CO}_3/\text{Co}_1\text{Mg}_2\text{Al}_1\text{O}_x$ , and 1 wt% Pt/15 wt%  $\text{K}_2\text{CO}_3/\text{Co}_1\text{Mg}_2\text{Al}_1\text{O}_x$  samples were also observed using SEM analyses, as shown in Fig. 6(b–d). It is apparent that after being calcined at 400 °C, the  $\text{Co}_1\text{Mg}_2\text{Al}_1\text{O}_x$  LDO still remained its “sand rose” morphology. After doping with  $\text{K}_2\text{CO}_3$ , the “sand rose” changed to plate-like nanoparticles, while after further doping with Pt, it changed into aggregates of spherical nanoparticles. To confirm the existence of Pt, HR-TEM images of 1 wt% Pt-15 wt%  $\text{K}_2\text{CO}_3/\text{Co}_1\text{Mg}_2\text{Al}_1\text{O}_x$  were also observed in Fig. 7(a) and (b). The Pt nanoparticles were clearly seen, suggesting that the Pt was highly dispersed in the sample.[42] The particle size distribution of Pt nanoparticles was shown in Fig. 7(c), indicating that the average particle size of Pt is 4–6 nm. The existence of Pt and K species was also confirmed by TEM-EDS analysis, as shown in Fig. 7(d). The elements of K, C, O, and Pt were detected, further confirming the existence of Pt and  $\text{K}_2\text{CO}_3$ .

The SSA of different LDOs, 15 wt%  $\text{K}_2\text{CO}_3/\text{Co}_1\text{Mg}_2\text{Al}_1\text{O}_x$ , and 1 wt% Pt/15 wt%  $\text{K}_2\text{CO}_3/\text{Co}_1\text{Mg}_2\text{Al}_1\text{O}_x$  were measured by the  $\text{N}_2$  adsorption and desorption at 77 K and calculated using the Brunauer–Emmett–Teller (BET) method, as shown in Table 1. All the  $\text{CoMgAlO}_x$  were obtained by calcining the corresponding  $\text{CoMgAl-CO}_3$  LDHs at 400 °C. It can be seen that all samples have a SSA between 160 and 330  $\text{m}^2/\text{g}$ . The highest surface areas correspond to the samples with a lower cobalt content ( $\text{Co}_{0.25}\text{Mg}_{2.75}\text{Al}_1\text{O}_x$ , 328.97  $\text{m}^2/\text{g}$ ).[25] After doping  $\text{K}_2\text{CO}_3$  and Pt onto  $\text{Co}_1\text{Mg}_2\text{Al}_1\text{O}_x$ , the surface area of 15 wt%  $\text{K}_2\text{CO}_3/\text{Co}_1\text{Mg}_2\text{Al}_1\text{O}_x$  and 1 wt% Pt-15 wt%  $\text{K}_2\text{CO}_3/\text{Co}_1\text{Mg}_2\text{Al}_1\text{O}_x$  decreased by some extent, which is possibly due to the partial pore blocking by the introduction of  $\text{K}_2\text{CO}_3$ .

In order to obtain the optimal loadings of Pt and  $K_2CO_3$ , the influences of Pt and  $K_2CO_3$  loadings on the  $NO_x$  storage capacity of  $Co_1Mg_2Al_1O_x$  were studied. Fig. 8(a) shows the effect of  $K_2CO_3$  loading. In general, the  $NO_x$  storage capacity of  $K_2CO_3$  promoted  $Co_1Mg_2Al_1O_x$  increased with the increase of  $K_2CO_3$  loadings. However, when the  $K_2CO_3$  loading reached 25 wt%, the overall  $NO_x$  storage capacity did not significantly change, indicating that the additional  $K_2CO_3$  could not provide further enhancement in the amount of stored  $NO_x$ . At 300 °C, the best  $K_2CO_3$  loading for  $Co_1Mg_2Al_1O_x$  is 15 wt%, with the  $NO_x$  storage capacity was increased from 0.50 to 1.05 mmol/g.

For efficient  $NO_x$  reduction, it is well known that Pt is required for the selective reduction of adsorbed  $NO_x$  in the presence of reducing agents.  $NO_x$  storage capacity on Pt doped  $Co_1Mg_2Al_1O_x$  was then investigated by isothermal storage of  $NO_x$  at 300 °C. For 1 wt% Pt/ $Co_1Mg_2Al_1O_x$  catalyst, the  $NO_x$  storage capacity is significantly enhanced, comparing to the undoped  $Co_1Mg_2Al_1O_x$ . However, as shown in Fig. 8(b), the  $NO_x$  storage capacity decreased with the increase in Pt loading, suggesting that 1 wt% was the optimal Pt loading. Furthermore, by co-doping 1 wt% Pt and 15 wt%  $K_2CO_3$ , the  $NO_x$  storage capacity of  $Co_1Mg_2Al_1O_x$  could be significantly improved to 1.2 mmol/g, as shown in Fig. 9(a). The  $NO_x$  storage capacities of  $Mg_3Al_1O_x$ ,  $Co_1Mg_2Al_1O_x$ , 1 wt% Pt/ $Co_1Mg_2Al_1O_x$ , 15 wt%  $K_2CO_3$ / $Co_1Mg_2Al_1O_x$ , and 1 wt% Pt/15 wt%  $K_2CO_3$ / $Co_1Mg_2Al_1O_x$  were summarized and compared in Fig. 9(a). It is apparent the capacity gradually increased after each modification. For instance, by introducing Co, the  $NO_x$  storage capacity was significantly increased from 0.14 mmol/g for  $Mg_3Al_1O_x$  to 0.50 mmol/g for  $Co_1Mg_2Al_1O_x$ . By further doing with 1 wt% Pt or 15 wt%  $K_2CO_3$ , the  $NO_x$  storage capacity was further increased to 0.60 and 1.04 mmol/g, respectively. Finally, with both 1 wt% Pt and 15 wt%  $K_2CO_3$ , the  $NO_x$

storage capacity can reach as high as 1.20 mmol/g. We also prepared a conventional 1 wt% Pt-20 wt% BaO/ $\gamma$ -Al<sub>2</sub>O<sub>3</sub> catalyst and tested its NO<sub>x</sub> storage capacities at different temperatures, as shown in Fig. S11. The highest NO<sub>x</sub> storage capacity of 1 wt% Pt-20 wt% BaO/ $\gamma$ -Al<sub>2</sub>O<sub>3</sub> was only 0.56 mmol/g at 300 °C, which is much less than that of our newly developed 1 wt% Pt/15 wt% K<sub>2</sub>CO<sub>3</sub>/Co<sub>1</sub>Mg<sub>2</sub>Al<sub>1</sub>O<sub>x</sub> catalyst. The data suggests that significant promoting effect could be achieved by proper designing the catalysts.

In order to have a comprehensive understanding of this novel catalyst (1 wt% Pt-15 wt% K<sub>2</sub>CO<sub>3</sub>/Co<sub>1</sub>Mg<sub>2</sub>Al<sub>1</sub>O<sub>x</sub>), its isothermal NO<sub>x</sub> storage performance at different temperatures ranging from 100 to 400 °C was also evaluated. As shown in Fig. 9(b), in the low temperature range (100–300 °C), the NO<sub>x</sub> storage capacity increases with the increase in adsorption temperature, and the highest NO<sub>x</sub> storage capacity of around 1.20 mmol/g was obtained at 300 °C. While, at 400 °C, the NO<sub>x</sub> storage capacity started to decrease, which was 0.98 mmol/g.

To further evaluate the reduction activity of adsorbed NO<sub>x</sub>, a lean–rich cycling test was carried out over 1 wt% Pt-15 wt% K<sub>2</sub>CO<sub>3</sub>/Co<sub>1</sub>Mg<sub>2</sub>Al<sub>1</sub>O<sub>x</sub> at 300 °C (Fig. 10). During lean periods, NO was first oxidized to NO<sub>2</sub> by Pt or Co-related phases, and NO<sub>2</sub> was then adsorbed on the catalyst. During rich periods, the adsorbed NO<sub>x</sub> reacted with reducing reagent (H<sub>2</sub>) in the presence of Pt. Fig. 10(b) suggests that the NO<sub>x</sub> was selectively reduced to N<sub>2</sub> and H<sub>2</sub>O during the rich cycles. Overall, more than 73% of NO<sub>x</sub> was removed during the lean–rich cycling tests. Its superior stability was further confirmed by its stable NSR performance during 9 lean–rich cycles.

### **3.4. The effect of CO<sub>2</sub>, SO<sub>2</sub>, and H<sub>2</sub>O on Pt-K<sub>2</sub>CO<sub>3</sub>/CoMgAlO<sub>x</sub>**

In naphtha crackers flue gases, CO<sub>2</sub> contributes more than 7% to the total exhaust, thus the CO<sub>2</sub> poisoning is considered in our paper. The CO<sub>2</sub> poisoning effect on the

NO<sub>x</sub> storage capacity of 1 wt% Pt-15 wt% K<sub>2</sub>CO<sub>3</sub>/Co<sub>1</sub>Mg<sub>2</sub>Al<sub>1</sub>O<sub>x</sub> was first studied in the presence of various amounts of CO<sub>2</sub> (6–10%) (Fig. 11(a)). When the CO<sub>2</sub> concentration was less than 9%, the CO<sub>2</sub> poisoning effect was not significant, and only a slight decrease in NO<sub>x</sub> storage amount was observed. The NO<sub>x</sub> adsorption capacity gradually decreased with increasing CO<sub>2</sub> concentration, indicating that CO<sub>2</sub> competes with NO<sub>x</sub> molecules for the adsorption sites. When the CO<sub>2</sub> concentration reached 10%, the NO<sub>x</sub> adsorption capacity decreased to 0.8 mmol/g.

Although the concentration of SO<sub>2</sub> is relatively low (< 1 ppm) in cracker flue gases, it is still necessary to study the influence of SO<sub>2</sub> on the NO<sub>x</sub> storage capacity of 1 wt% Pt-15 wt% K<sub>2</sub>CO<sub>3</sub>/Co<sub>1</sub>Mg<sub>2</sub>Al<sub>1</sub>O<sub>x</sub>, which is of great practical importance. In this contribution, a much higher SO<sub>2</sub> concentration of 5–30 ppm was utilized to observe the accelerated poisoning effect on the catalyst. Fig. 11(b) shows that with the increase in SO<sub>2</sub> concentration, the NO<sub>x</sub> storage capacity decreased by certain extent. With 5, 10, and 30 ppm SO<sub>2</sub>, the NO<sub>x</sub> storage capacity decreased from 1.2 to 0.95, 0.85, and 0.74 mmol/g, respectively. Considering the fact that the actual SO<sub>2</sub> concentration in naphtha cracker flue gases is normally only 0.1–0.3 ppm, the influence of SO<sub>2</sub> is not considered as a problem for this new NSR catalyst.

In addition to CO<sub>2</sub> and SO<sub>2</sub>, the effect of 5% H<sub>2</sub>O on the NO<sub>x</sub> storage capacity of 1 wt% Pt-15 wt% K<sub>2</sub>CO<sub>3</sub>/Co<sub>1</sub>Mg<sub>2</sub>Al<sub>1</sub>O<sub>x</sub> was also studied. Fig. S12 shows the isothermal NO<sub>x</sub> storage performance of 1 wt% Pt-15 wt% K<sub>2</sub>CO<sub>3</sub>/Co<sub>1</sub>Mg<sub>2</sub>Al<sub>1</sub>O<sub>x</sub> catalyst at 300 °C with and without 5% H<sub>2</sub>O. After adding 5% H<sub>2</sub>O, the NO<sub>x</sub> storage capacity of 1 wt% Pt-15 wt% K<sub>2</sub>CO<sub>3</sub>/Co<sub>1</sub>Mg<sub>2</sub>Al<sub>1</sub>O<sub>x</sub> only slightly decreased from 1.20 to 1.02 mmol/g, suggesting that this novel catalyst is also resistant to water vapor.

#### 4. Conclusion

In this contribution, a range of binary LDHs synthesized using AMOST method including  $\text{Ca}_2\text{Al}_1\text{-NO}_3$ ,  $\text{Zn}_3\text{Al}_1\text{-CO}_3$ ,  $\text{Cu}_3\text{Al}_1\text{-CO}_3$ ,  $\text{Co}_3\text{Al}_1\text{-CO}_3$ ,  $\text{Ni}_3\text{Al}_1\text{-CO}_3$ , and  $\text{Mg}_3\text{Al}_1\text{-CO}_3$  were systematically investigated as precursors for the preparation of efficient  $\text{NO}_x$  storage materials. The results indicated that the  $\text{Zn}_3\text{Al}_1\text{O}_x$ ,  $\text{Cu}_3\text{Al}_1\text{O}_x$ , and  $\text{Ca}_2\text{Al}_1\text{O}_x$  LDOs adsorb  $\text{NO}_x$  at relatively low temperatures (90–150 °C) but their  $\text{NO}_x$  storage capacities are much lower than other LDOs. We found the optimal  $\text{NO}_x$  adsorption temperature range for  $\text{Ni}_3\text{Al}_1\text{O}_x$ ,  $\text{Co}_3\text{Al}_1\text{O}_x$ , and  $\text{Mg}_3\text{Al}_1\text{O}_x$  is 120–250 °C, 150–180 °C, and 400 °C respectively. For these materials their  $\text{NO}_x$  storage capacities were much improved, ca. 0.21–0.26 mmol/g. Different LDOs also showed different NO oxidation abilities. The thermal stability of  $\text{NO}_x$  adsorbed on the LDOs follows the order  $\text{Mg}_3\text{Al}_1\text{O}_x > \text{Ni}_3\text{Al}_1\text{O}_x > \text{Cu}_3\text{Al}_1\text{O}_x > \text{Co}_3\text{Al}_1\text{O}_x$ , with the peak desorption temperatures of 500, 390, 320, and 290 °C respectively. Thus by combining the merits of Co and Mg, a ternary LDO derived from  $\text{CoMgAl-CO}_3$  with different Co/Mg ratios were designed, which showed much improved  $\text{NO}_x$  storage capacity. The optimal ternary LDO was determined to be  $\text{Co}_1\text{Mg}_2\text{Al}_1\text{O}_x$ , with a  $\text{NO}_x$  storage capacity of ca. 0.50 mmol/g at 300 °C. By doping Pt and  $\text{K}_2\text{CO}_3$ , a novel NSR catalyst 1 wt% Pt/15 wt%  $\text{K}_2\text{CO}_3/\text{Co}_1\text{Mg}_2\text{Al}_1\text{O}_x$  was developed, and the  $\text{NO}_x$  storage capacity was further improved to as high as 1.2 mmol/g, which is much higher than the traditional Pt-BaO/ $\gamma$ - $\text{Al}_2\text{O}_3$  (0.56 mmol/g).  $\text{NO}_x$  storage and reduction cycling tests demonstrated that this adsorbent had a good stability after 9 cycles. This new NSR catalyst also demonstrates relatively good  $\text{CO}_2$  and  $\text{SO}_2$  resistance, suggesting significant potential for use for  $\text{NO}_x$  emission control from naphtha cracker flue gases.

## Acknowledgment

The authors thank the Fundamental Research Funds for the Central Universities

(2016ZCQ03), the National Natural Science Foundation of China (51622801, 51572029), the Beijing Excellent Young Scholar (2015000026833ZK11), and SCG Chemicals Co Ltd, Thailand for financial support.

## References

- [1] O. Tokunaga, N. Suzuki, Radiation chemical reactions in NO<sub>x</sub> and SO<sub>2</sub> removals from flue gas, *Radiat. Phys. Chem.*, 24 (1984) 145.
- [2] O.M. Bade, J.N. Knudsen, O. Gorset, I. Skestad, Controlling amine mist formation in CO<sub>2</sub> capture from Residual Catalytic Cracker (RCC) flue gas, *Energy Proced.*, 63 (2014) 884
- [3] A. Pawelec, A.G. Chmielewski, J. Licki, B. Han, J. Kim, N. Kunnummal, O.I. Fageeh, Pilot plant for electron beam treatment of flue gases from heavy fuel oil fired boiler, *Fuel Process. Technol.*, 145 (2016) 123.
- [4] N. Takahashi, H. Shinjoh, T. Iijima, T. Suzuki, K. Yamazaki, K. Yokota, H. Suzuki, N. Miyoshi, S. Matsumoto, T. Tanizawa, T. Tanaka, S. Tateishi, K. Kasahara, The new concept 3-way catalyst for automotive lean-burn engine: NO<sub>x</sub> storage and reduction catalyst, *Catal. Today*, 27 (1996) 63.
- [5] I. Nova, L. Castoldi, L. Lietti, E. Tronconi, P. Forzatti, F. Prinetto, G. Ghiotti, NO<sub>x</sub> adsorption study over Pt–Ba/alumina catalysts: FT-IR and pulse experiments, *J. Catal.*, 222 (2004) 377.
- [6] H. Imagawa, T. Tanaka, N. Takahashi, S. Matsunaga, A. Suda, H. Shinjoh, Titanium-doped nanocomposite of Al<sub>2</sub>O<sub>3</sub> and ZrO<sub>2</sub>–TiO<sub>2</sub> as a support with high sulfur durability for NO<sub>x</sub> storage-reduction catalyst, *Appl. Catal. B: Environ.*, 86 (2009) 63.
- [7] I. Malpartida, M. Vargas, L. Alemany, E. Finocchio, G. Busca, Pt–Ba–Al<sub>2</sub>O<sub>3</sub> for NO<sub>x</sub> storage and reduction: characterization of the dispersed species, *Appl. Catal. B: Environ.*, 80 (2008) 214.
- [8] W. Epling, A. Yezerets, N. Currier, The effects of regeneration conditions on NO<sub>x</sub> and NH<sub>3</sub> release from NO<sub>x</sub> storage/reduction catalysts, *Appl. Catal. B: Environ.*, 74 (2007) 117.
- [9] T. Lesage, J. Saussey, S. Malo, M. Hervieu, C. Hedouin, G. Blanchard, M. Daturi, Operando FTIR study of NO<sub>x</sub> storage over a Pt/K/Mn/Al<sub>2</sub>O<sub>3</sub>–CeO<sub>2</sub> catalyst, *Appl. Catal. B: Environ.*, 72 (2007) 166.
- [10] M. Piacentini, M. Maciejewski, A. Baiker, NO<sub>x</sub> storage-reduction behavior of Pt–Ba/MO<sub>2</sub> (MO<sub>2</sub> = SiO<sub>2</sub>, CeO<sub>2</sub>, ZrO<sub>2</sub>) catalysts, *Appl. Catal. B: Environ.*, 72 (2007) 105.
- [11] Q. Wang, J. Sohn, J. Chung, Thermally stable Pt/K<sub>2</sub>Ti<sub>2</sub>O<sub>5</sub> as high-temperature NO<sub>x</sub> storage and reduction catalyst, *Appl. Catal. B: Environ.*, 89 (2009) 97.
- [12] Q. Wang, J. Chung, NO<sub>x</sub> storage and reduction over Cu/K<sub>2</sub>Ti<sub>2</sub>O<sub>5</sub> in a wide temperature range: activity, characterization, and mechanism, *Appl. Catal. A: Gen.*, 358 (2009) 59.

- [13] S. Matsumoto, Y. Ikeda, H. Suzuki, M. Ogai, NO<sub>x</sub> storage-reduction catalyst for automotive exhaust with improved tolerance against sulfur poisoning, *Appl. Catal. B: Environ.*, 25 (2000) 115.
- [14] K. Yamazaki, T. Suzuki, N. Takahashi, K. Yokota, M. Sugiura, Effect of the addition of transition metals to Pt/Ba/Al<sub>2</sub>O<sub>3</sub> catalyst on the NO<sub>x</sub> storage-reduction catalysis under oxidizing conditions in the presence of SO<sub>2</sub>, *Appl. Catal. B: Environ.*, 30 (2001) 459.
- [15] A. Lindholm, N. Currier, E. Fridell, A. Yezerets, L. Olsson, NO<sub>x</sub> storage and reduction over Pt based catalysts with hydrogen as the reducing agent: Influence of H<sub>2</sub>O and CO<sub>2</sub>, *Appl. Catal. B: Environ.*, 75 (2007) 78.
- [16] F. Garin, Mechanism of NO<sub>x</sub> decomposition, *Appl. Catal. A: Gen.*, 222 (2001) 183.
- [17] A. Sultana, D. Habermacher, C. Kirschhock, J. Martens, Adsorptive separation of NO<sub>x</sub> in presence of SO<sub>x</sub> from gas mixtures simulating lean burn engine exhaust by pressure swing process on Na–Y zeolite, *Appl. Catal. B: Environ.*, 48 (2004) 65.
- [18] J. Luo, M. Meng, Y. Zha, Y. Xie, T. Hu, J. Zhang, T. Liu, A comparative study of Pt/Ba/Al<sub>2</sub>O<sub>3</sub> and Pt/Fe-Ba/Al<sub>2</sub>O<sub>3</sub> NSR catalysts: New insights into the interaction of Pt-Ba and the function of Fe, *Appl. Catal. B: Environ.*, 78 (2008) 38.
- [19] G. Centi, G. Arena, S. Perathoner, Nanostructured catalysts for NO<sub>x</sub> storage–reduction and N<sub>2</sub>O decomposition, *J. Catal.*, 216 (2003) 443.
- [20] G. Fornasari, F. Trifirò, A. Vaccari, F. Prinetto, G. Ghiotti, G. Centi, Novel low temperature NO<sub>x</sub> storage-reduction catalysts for diesel light-duty engine emissions based on hydrotalcite compounds, *Catal. Today*, 75 (2002) 421.
- [21] S. Hodjati, K. Vaezzadeh, C. Petit, V. Pitchon, A. Kiennemann, Absorption/desorption of NO<sub>x</sub> process on perovskites: performances to remove NO<sub>x</sub> from a lean exhaust gas, *Appl. Catal. B: Environ.*, 26 (2000) 5.
- [22] A.J. Ma, S.Z. Wang, C. Liu, H. Xian, Q. Ding, L. Guo, M. Meng, Y.S. Tan, N. Tsubaki, J. Zhang, L.R. Zheng, X.G. Li, Effects of Fe dopants and residual carbonates on the catalytic activities of the perovskite-type La<sub>0.7</sub>Sr<sub>0.3</sub>Co<sub>1-x</sub>Fe<sub>x</sub>O<sub>3</sub> NO<sub>x</sub> storage catalyst, *Appl. Catal. B: Environ.*, 146 (2014) 24.
- [23] R. You, Y. Zhang, D. Liu, M. Meng, Z. Jiang, S. Zhang, Y. Huang, A series of ceria supported lean-burn NO<sub>x</sub> trap catalysts LaCoO<sub>3</sub>/K<sub>2</sub>CO<sub>3</sub>/CeO<sub>2</sub> using perovskite as active component, *Chem. Eng. J.*, 260 (2015) 357.
- [24] Q. Wang, Z. Guo, J.S. Chung, Molecular NO<sub>2</sub> induced K<sub>2</sub>Ti<sub>2</sub>O<sub>5</sub>–K<sub>2</sub>Ti<sub>6</sub>O<sub>13</sub> structure switching in the dry gas phase: lattice potassium reactivity, *Chem. Commun.*, (2009) 5284.
- [25] J.J. Yu, Z. Jiang, L. Zhu, Z.P. Hao, Z.P. Xu, Adsorption/desorption studies of NO<sub>x</sub> on well-mixed oxides derived from Co-Mg/Al hydrotalcite-like compounds., *J. Phys. Chem. B*, 110 (2006) 4291.
- [26] Q. Wang, D. O'Hare, Recent advances in the synthesis and application of layered double hydroxide (LDH) nanosheets, *Chem. Rev.*, 112 (2012) 4124.
- [27] F. Cavani, F. Trifirò, A. Vaccari, Hydrotalcite-type anionic clays: preparation, properties and applications, *Catal. Today*, 11 (1991) 173.
- [28] Q. Wang, X. Zhang, J. Zhu, Z. Guo, D. O'Hare, Preparation of stable dispersions

of layered double hydroxides (LDHs) in nonpolar hydrocarbons: new routes to polyolefin/LDH nanocomposites, *Chem. Commun.*, 48 (2012) 7450.

[29] Q. Wang, D. O'Hare, Large-scale synthesis of highly dispersed layered double hydroxide powders containing delaminated single layer nanosheets, *Chem. Commun.*, 49 (2013) 6301.

[30] C. Chen, M. Yang, Q. Wang, J.-C. Buffet, D. O'Hare, Synthesis and characterisation of aqueous miscible organic-layered double hydroxides, *J. Mater. Chem. A*, 2 (2014) 15102.

[31] M. Konsolakis, I. Yentekakis, Strong promotional effects of Li, K, Rb and Cs on the Pt-catalysed reduction of NO by propene, *Appl. Catal. B: Environ.*, 29 (2001) 103.

[32] N. Takahashi, S. Matsunaga, T. Tanaka, H. Sobukawa, H. Shinjoh, New approach to enhance the NO<sub>x</sub> storage performance at high temperature using basic MgAl<sub>2</sub>O<sub>4</sub> spinel support, *Appl. Catal. B: Environ.*, 77 (2007) 73.

[33] Z. Zhang, J. Wang, L. Huang, Y. Gao, A. Umar, Z. Huang, Q. Wang, The influence of synthesis method on the CO<sub>2</sub> adsorption capacity of Mg<sub>3</sub>Al-CO<sub>3</sub> hydrotalcite-derived adsorbents, *Sci. Adv. Mater.*, 6 (2014) 1154.

[34] Q. Wang, Y. Gao, Z. Zhang, L. Duan, A. Umar, D. O'Hare, Synthesis and characterization of high surface area flower-like Ca-containing layered double hydroxides Mg<sub>3-x</sub>Ca<sub>x</sub>Al<sub>1</sub>-NO<sub>3</sub>, *Sci. Adv. Mater.*, 5 (2013) 411.

[35] B.A. Silletti, R.T. Adams, S.M. Sigmon, A. Nikolopoulos, J.J. Spivey, H.H. Lamb, A novel Pd/MgAlO<sub>x</sub> catalyst for NO<sub>x</sub> storage-reduction, *Catal. Today*, 114 (2006) 64.

[36] Q. Wang, J. Luo, Z. Zhong, A. Borgna, CO<sub>2</sub> capture by solid adsorbents and their applications: current status and new trends, *Energy Environ. Sci.*, 4 (2011) 42.

[37] Q. Wang, H.H. Tay, D.J.W. Ng, L. Chen, Y. Liu, J. Chang, Z. Zhong, J. Luo, A. Borgna, The effect of trivalent cations on the performance of Mg-M-CO<sub>3</sub> layered double hydroxides for high-temperature CO<sub>2</sub> capture, *ChemSusChem* 3(2010) 965.

[38] J. Wang, X. Mei, L. Huang, Q. Zheng, Y. Qiao, K. Zang, S. Mao, R. Yang, Z. Zhang, Y. Gao, Z. Guo, Z. Huang, Q. Wang, Synthesis of layered double hydroxides/graphene oxide nanocomposite as a novel high-temperature CO<sub>2</sub> adsorbent, *J. Energy Chem.*, 24 (2015) 127.

[39] Q. Wang, H.H. Tay, Z. Guo, L. Chen, Y. Liu, J. Chang, Z. Zhong, J. Luo, A. Borgna, Morphology and composition controllable synthesis of Mg-Al-CO<sub>3</sub> hydrotalcites by tuning the synthesis pH and the CO<sub>2</sub> capture capacity, *Appl. Clay Sci.*, 55 (2012) 18.

[40] R. Büchel, R. Strobel, A. Baiker, S.E. Pratsinis, Effect of the proximity of Pt to Ce or Ba in Pt/Ba/CeO<sub>2</sub> catalysts on NO<sub>x</sub> storage-reduction performance, *Top. Catal.*, 52 (2009) 1709.

[41] F. Prinetto, M. Manzoli, S. Morandi, F. Frola, G. Ghiotti, L. Castoldi, L. Lietti, P. Forzatti, Pt-K/Al<sub>2</sub>O<sub>3</sub> NSR catalysts: characterization of morphological, structural and surface properties, *J. Phys. Chem. C*, 114 (2009) 1127.

[42] X. Mei, J. Wang, R. Yang, Q. Yan, Q. Wang, Synthesis of Pt doped Mg-Al layered double oxide/graphene oxide hybrid as novel NO<sub>x</sub> storage-reduction catalyst, *RSC Adv.*, 5 (2015) 78061.

**Table 1.** SSA, pore size, and pore volume of different CoMgAlO<sub>x</sub> LDOs, 15 wt% K<sub>2</sub>CO<sub>3</sub>/Co<sub>1</sub>Mg<sub>2</sub>Al<sub>1</sub>O<sub>x</sub>, and 1 wt% Pt/15 wt% K<sub>2</sub>CO<sub>3</sub>/Co<sub>1</sub>Mg<sub>2</sub>Al<sub>1</sub>O<sub>x</sub>.

<b>LDOs</b>	<b>SSA (m<sup>2</sup>/g)</b>	<b>Pore size (Å)</b>	<b>Pore volume (cm<sup>3</sup>/g)</b>
Co <sub>0.25</sub> Mg <sub>2.75</sub> Al <sub>1</sub> O <sub>x</sub>	329.0	72.8	1.17
Co <sub>0.5</sub> Mg <sub>2.5</sub> Al <sub>1</sub> O <sub>x</sub>	311.6	63.9	1.35
Co <sub>1</sub> Mg <sub>2</sub> Al <sub>1</sub> O <sub>x</sub>	243.3	91.5	1.34
Co <sub>1.5</sub> Mg <sub>1.5</sub> Al <sub>1</sub> O <sub>x</sub>	188.5	88.0	1.10
Co <sub>2</sub> Mg <sub>1</sub> Al <sub>1</sub> O <sub>x</sub>	161.3	127.2	1.22
Co <sub>3</sub> Al <sub>1</sub> O <sub>x</sub>	122.5	218.1	0.70
15 wt% K <sub>2</sub> CO <sub>3</sub> /Co <sub>1</sub> Mg <sub>2</sub> Al <sub>1</sub> O <sub>x</sub>	159.1	79.9	0.85
1 wt% Pt/15 wt% K <sub>2</sub> CO <sub>3</sub> /Co <sub>1</sub> Mg <sub>2</sub> Al <sub>1</sub> O <sub>x</sub>	148.3	81.3	0.80

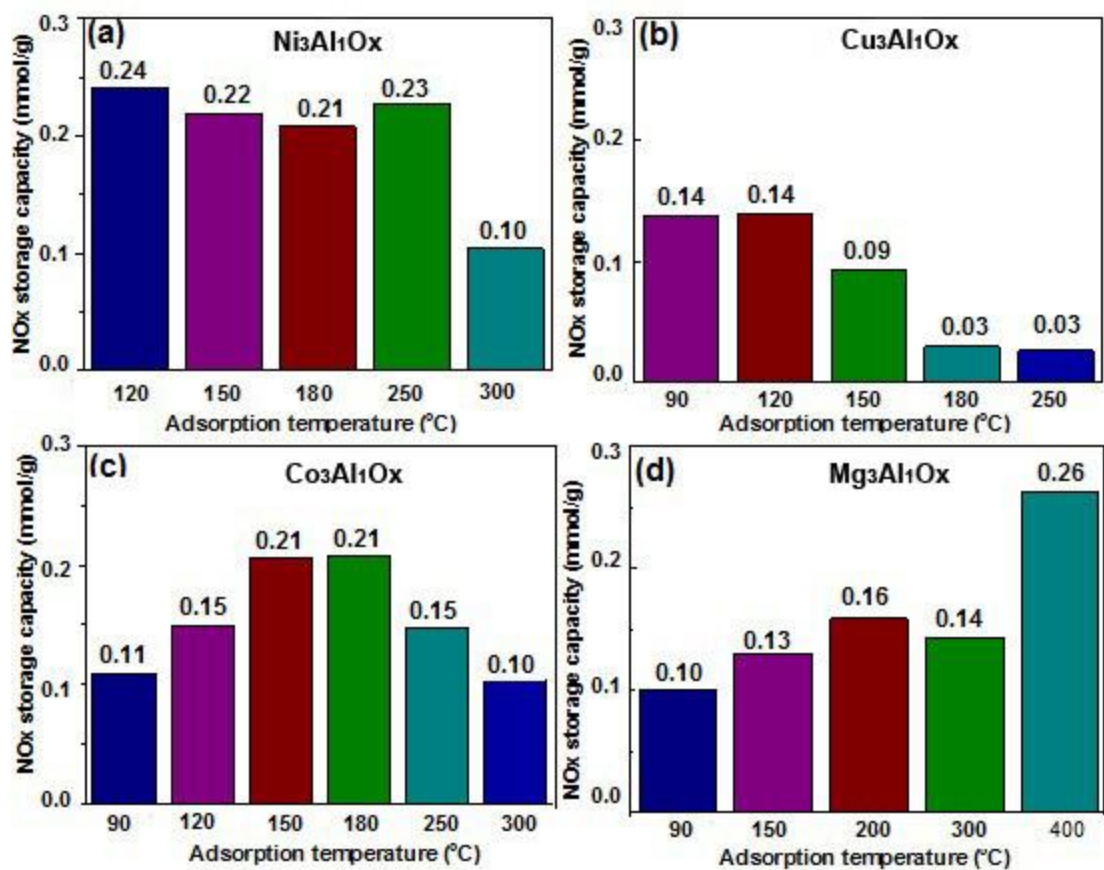


**Fig. 1.** NO<sub>x</sub> storage capacities of Ni<sub>3</sub>Al<sub>1</sub>O<sub>x</sub>, (b) Cu<sub>3</sub>Al<sub>1</sub>O<sub>x</sub>, (c) Co<sub>3</sub>Al<sub>1</sub>O<sub>x</sub>, and (d) Mg<sub>3</sub>Al<sub>1</sub>O<sub>x</sub> LDOs at different adsorption temperatures. Testing condition: 0.3 g catalyst (calcined at 400 °C, 5 h), 300 mL/min, 10% O<sub>2</sub>, and 100 ppm NO<sub>x</sub>.

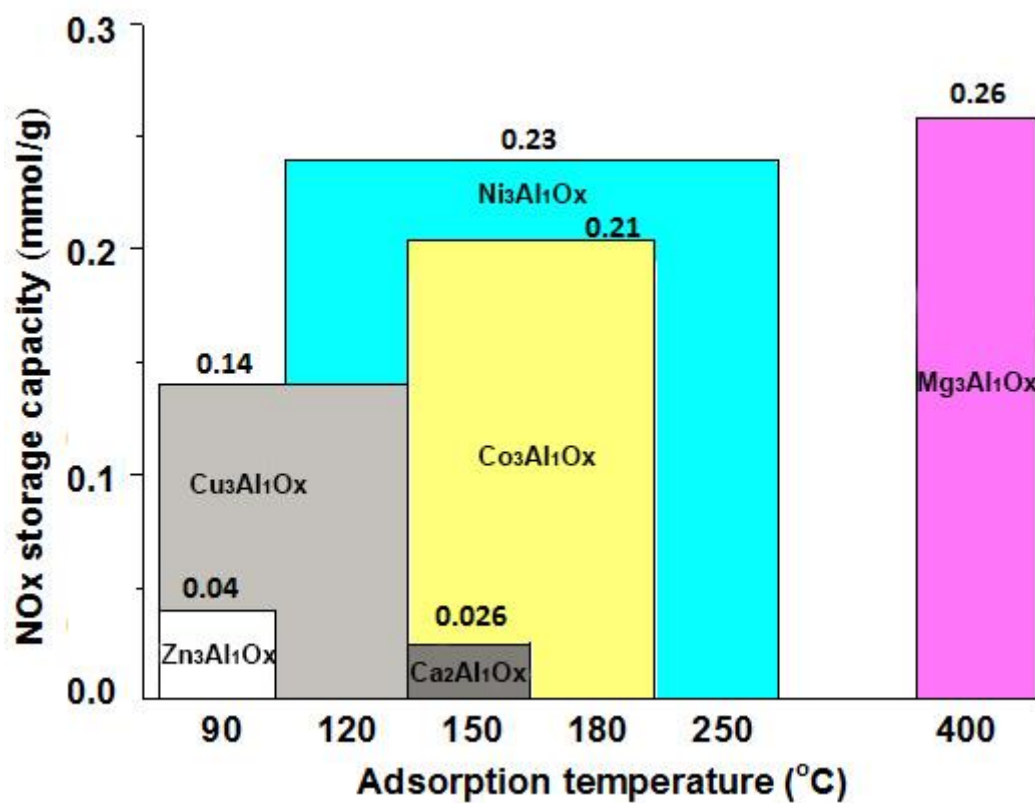


**Fig. 2.** The optimal NO<sub>x</sub> adsorption temperature range and their corresponding NO<sub>x</sub> storage capacities of different LDHs derived LDOs.

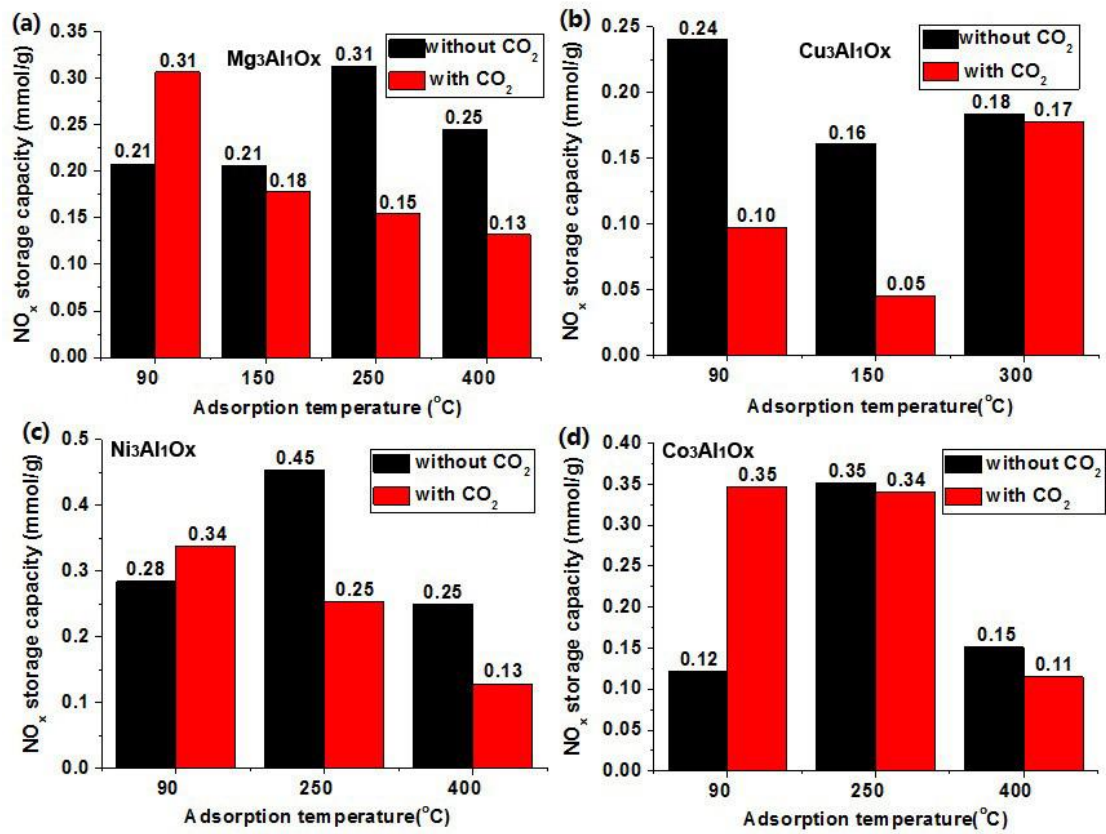


**Fig. 3.** The influence of 9%  $\text{CO}_2$  on the  $\text{NO}_x$  storage capacity of various LDOs at different temperatures (90–400 °C), (a)  $\text{Mg}_3\text{Al}_1\text{O}_x$ , (b)  $\text{Cu}_3\text{Al}_1\text{O}_x$ , (c)  $\text{Ni}_3\text{Al}_1\text{O}_x$ , and (d)  $\text{Co}_3\text{Al}_1\text{O}_x$ .

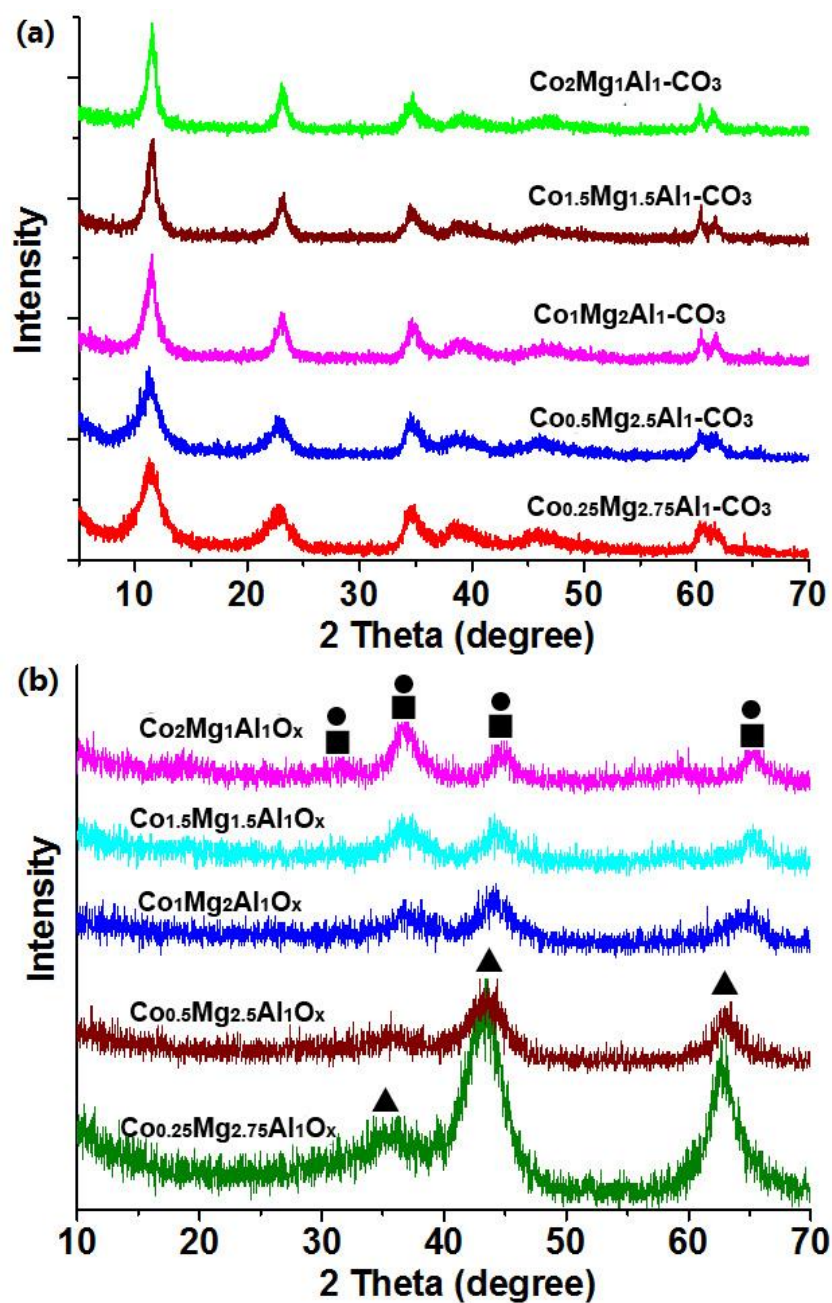


**Fig. 4.** (a) XRD patterns of fresh  $\text{Co}_x\text{Mg}_{3-x}\text{Al}_1\text{-CO}_3$  LDHs synthesized with different Co/Mg ratios, (b) XRD patterns of calcined  $\text{Co}_x\text{Mg}_{3-x}\text{Al}_1\text{-CO}_3$  LDHs at 400 °C. (■)  $\text{Co}_3\text{O}_4$ , (●)  $\text{CoAl}_2\text{O}_4$ , and (▲) periclase  $\text{MgO}$ .

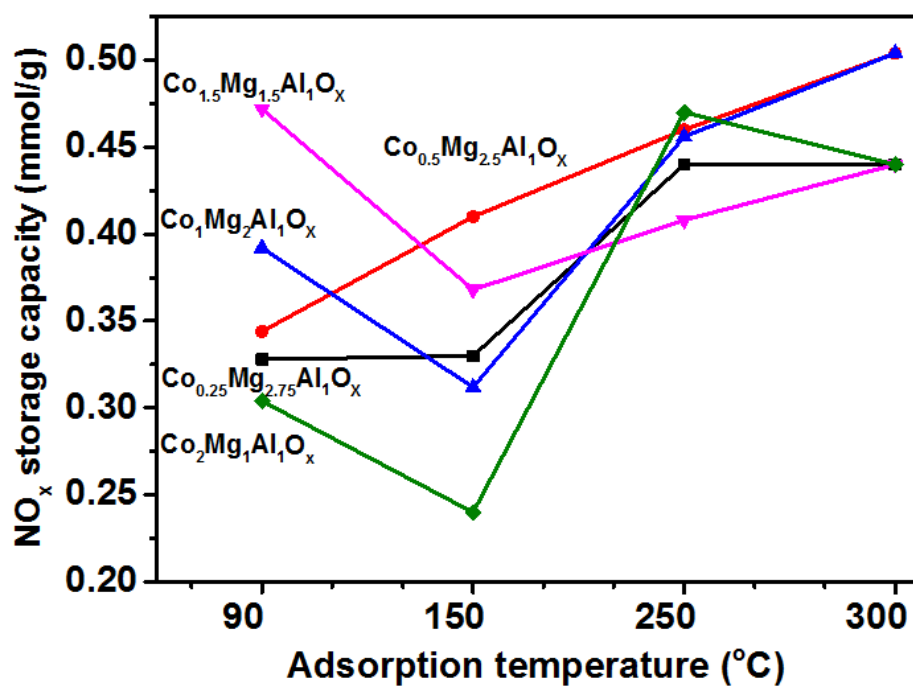


**Fig. 5.**  $\text{NO}_x$  storage capacity of  $\text{Co}_{0.25}\text{Mg}_{2.75}\text{Al}_1\text{O}_x$ ,  $\text{Co}_1\text{Mg}_2\text{Al}_1\text{O}_x$ ,  $\text{Co}_{1.5}\text{Mg}_{1.5}\text{Al}_1\text{O}_x$ , and  $\text{Co}_2\text{Mg}_1\text{Al}_1\text{O}_x$  at different temperatures. Testing condition: 0.2 g catalyst (calcined at 400 °C, 5 h), 300 mL/min (Ar: 270 mL/min,  $\text{O}_2$ : 30 mL/min), and 100 ppm  $\text{NO}_x$ .

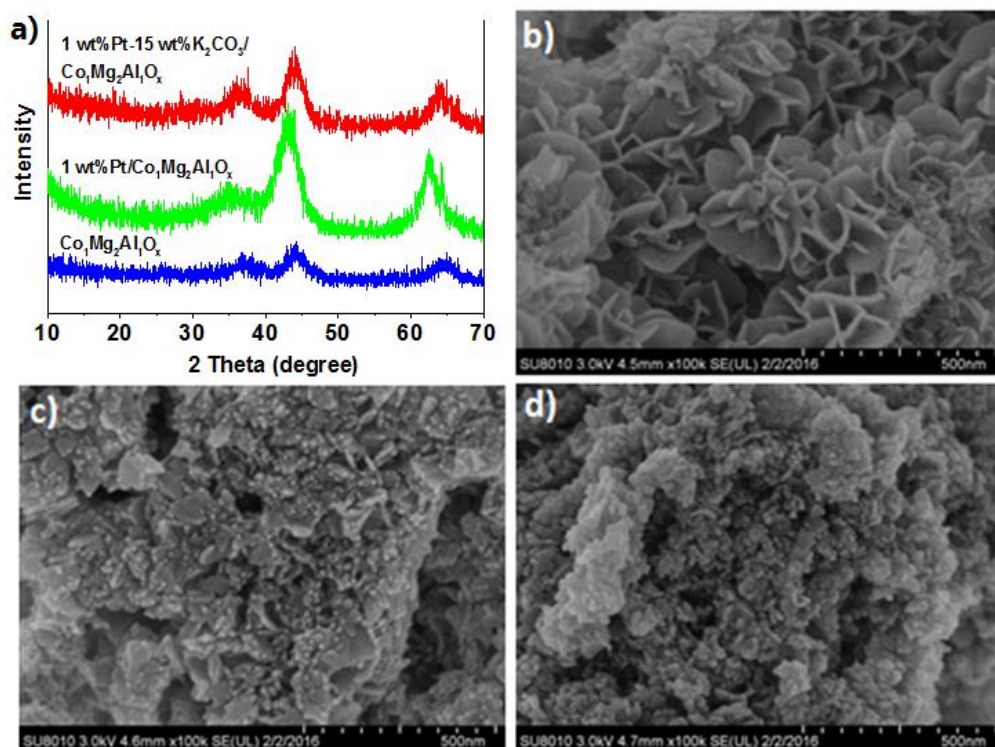


**Fig. 6.** (a) XRD patterns of Co<sub>1</sub>Mg<sub>2</sub>Al<sub>1</sub>O<sub>x</sub>, 1 wt% Pt/Co<sub>1</sub>Mg<sub>2</sub>Al<sub>1</sub>O<sub>x</sub>, and 1 wt% Pt-15 wt% K<sub>2</sub>CO<sub>3</sub>/Co<sub>1</sub>Mg<sub>2</sub>Al<sub>1</sub>O<sub>x</sub>. FE-SEM images of (b) Co<sub>1</sub>Mg<sub>2</sub>Al<sub>1</sub>O<sub>x</sub> LDO, (c) 15 wt% K<sub>2</sub>CO<sub>3</sub>/Co<sub>1</sub>Mg<sub>2</sub>Al<sub>1</sub>O<sub>x</sub>, (d) 1 wt% Pt-15 wt% K<sub>2</sub>CO<sub>3</sub>/Co<sub>1</sub>Mg<sub>2</sub>Al<sub>1</sub>O<sub>x</sub>.

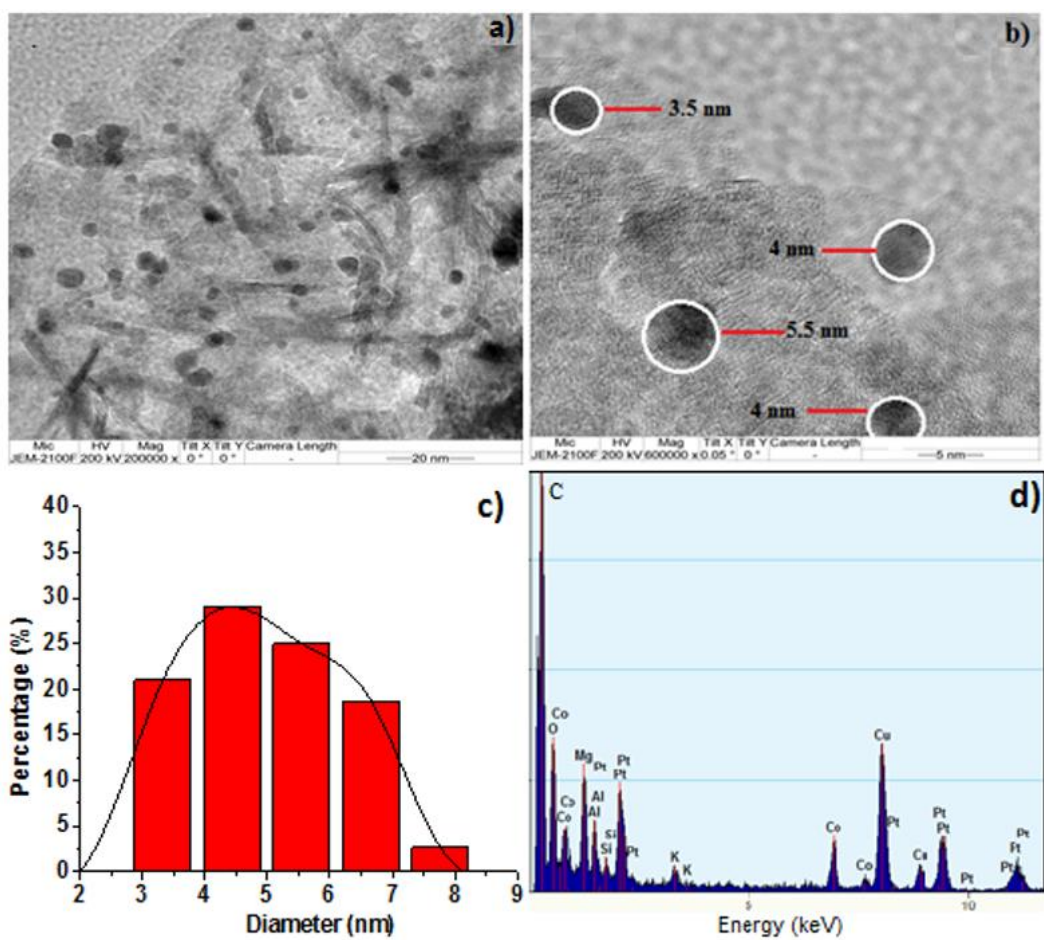


**Fig. 7.** (a, b) HR-TEM images, (c) the particle size distribution of Pt nanoparticles, and (d) TEM-EDS analysis of 1 wt% Pt-15 wt%  $\text{K}_2\text{CO}_3/\text{Co}_1\text{Mg}_2\text{Al}_1\text{O}_x$ .

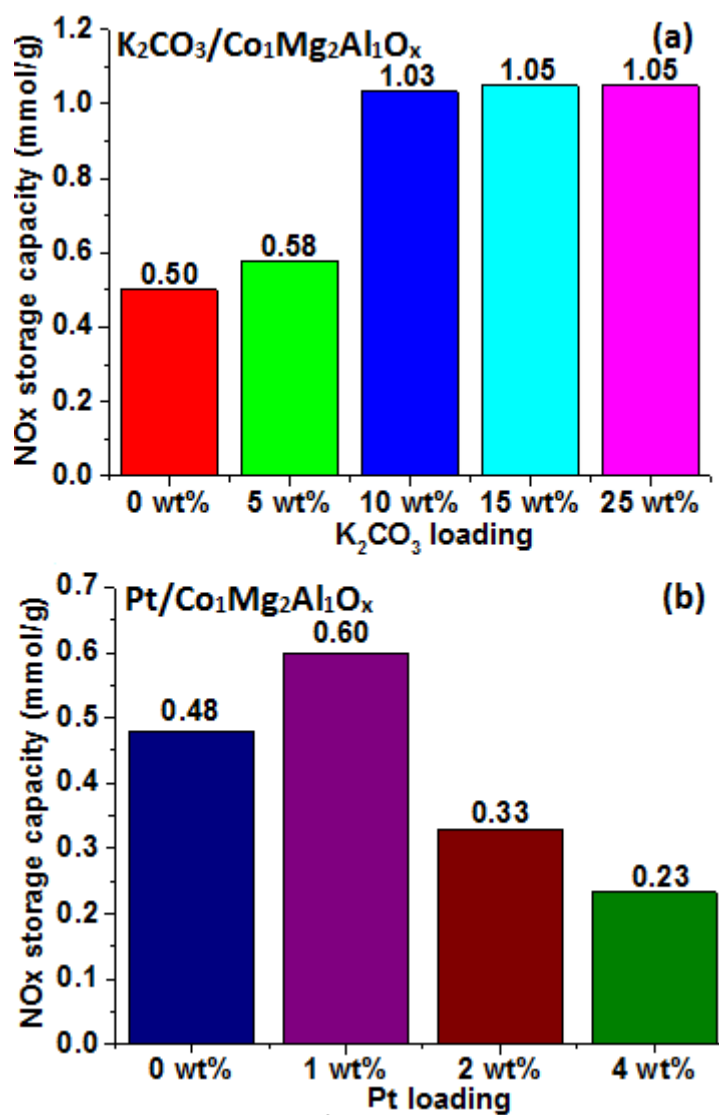


**Fig. 8.** (a) Isothermal NO<sub>x</sub> storage of  $K_2CO_3/Co_1Mg_2Al_1O_x$  with different  $K_2CO_3$  loadings, (b) Isothermal NO<sub>x</sub> storage of  $Pt/Co_1Mg_2Al_1O_x$  with different Pt loadings. Testing condition: 0.1 g doped catalyst or 0.2 g undoped catalyst (all samples were calcined at 400 °C, 5 h), 300 mL/min (Ar: 270 mL/min, O<sub>2</sub>: 30 mL/min), 100 ppm NO<sub>x</sub>.

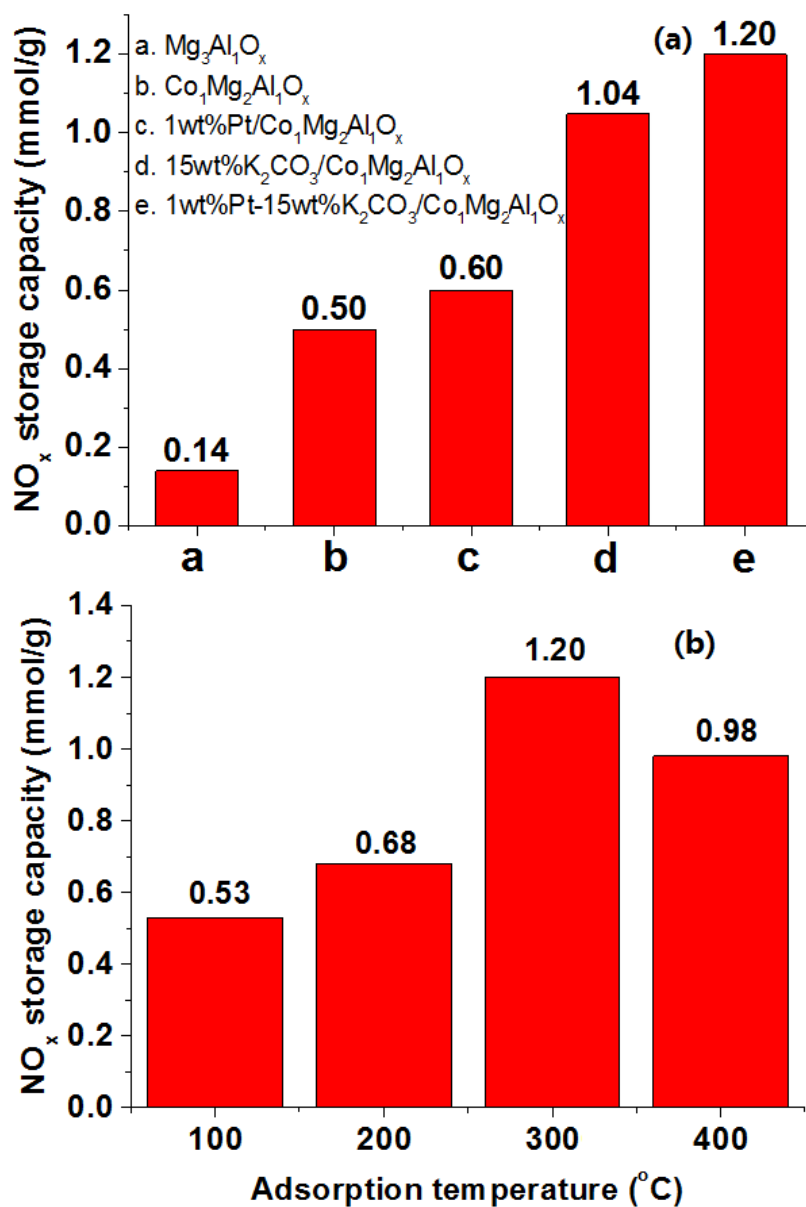


**Fig. 9.** (a) The NO<sub>x</sub> storage capacities of Mg<sub>3</sub>Al<sub>1</sub>O<sub>x</sub>, Co<sub>1</sub>Mg<sub>2</sub>Al<sub>1</sub>O<sub>x</sub>, 1 wt% Pt/Co<sub>1</sub>Mg<sub>2</sub>Al<sub>1</sub>O<sub>x</sub>, 15 wt% K<sub>2</sub>CO<sub>3</sub>/Co<sub>1</sub>Mg<sub>2</sub>Al<sub>1</sub>O<sub>x</sub>, and 1 wt% Pt-15 wt% K<sub>2</sub>CO<sub>3</sub>/Co<sub>1</sub>Mg<sub>2</sub>Al<sub>1</sub>O<sub>x</sub>. (b) Isothermal storage of NO<sub>x</sub> on 1 wt% Pt-15 wt% K<sub>2</sub>CO<sub>3</sub>/Co<sub>1</sub>Mg<sub>2</sub>Al<sub>1</sub>O<sub>x</sub> at 100, 200, 300, and 400 °C. Testing condition: 0.05 g catalyst (calcined at 400 °C, 5 h), 300 mL/min (Ar: 270 mL/min, O<sub>2</sub>: 30 mL/min), 100 ppm NO<sub>x</sub>.

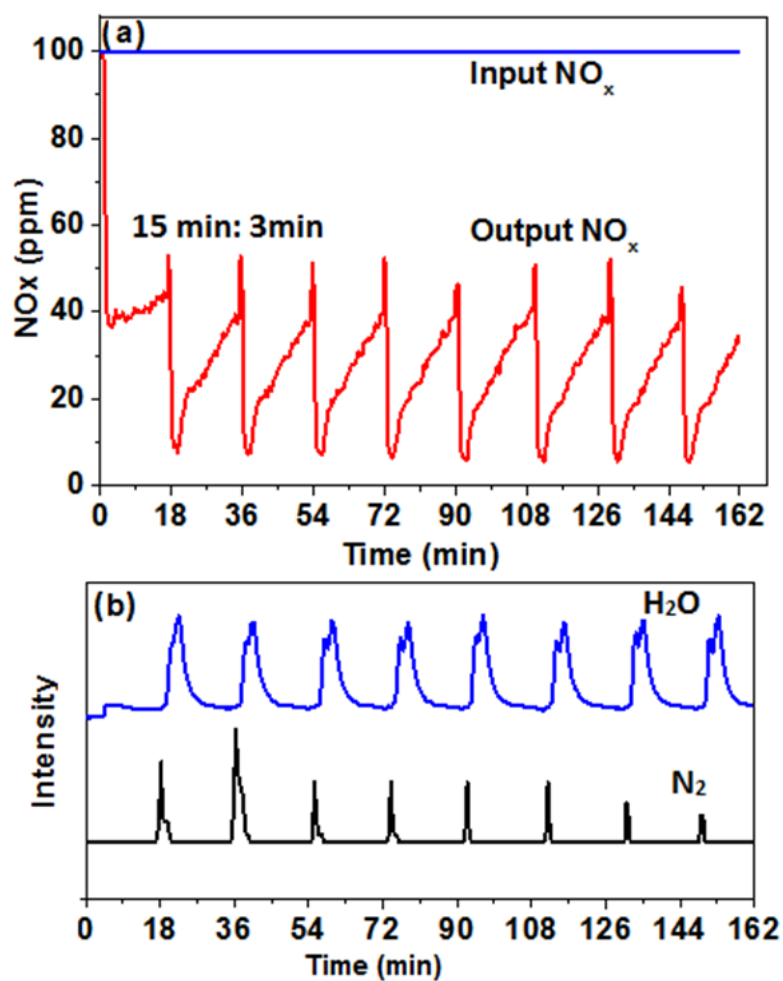


**Fig. 10.** Evolutions of NO<sub>x</sub>, H<sub>2</sub>O, and N<sub>2</sub> during 9 lean-rich cycling tests over 1 wt% Pt-15 wt% K<sub>2</sub>CO<sub>3</sub>/Co<sub>1</sub>Mg<sub>2</sub>Al<sub>1</sub>O<sub>x</sub> at 300 °C. Lean condition: 100 ppm NO<sub>x</sub>, 10% O<sub>2</sub>, 300 mL/min, Ar balanced; rich condition: 100 ppm NO<sub>x</sub>, 3.5% H<sub>2</sub>, 300 mL/min, Ar balanced.

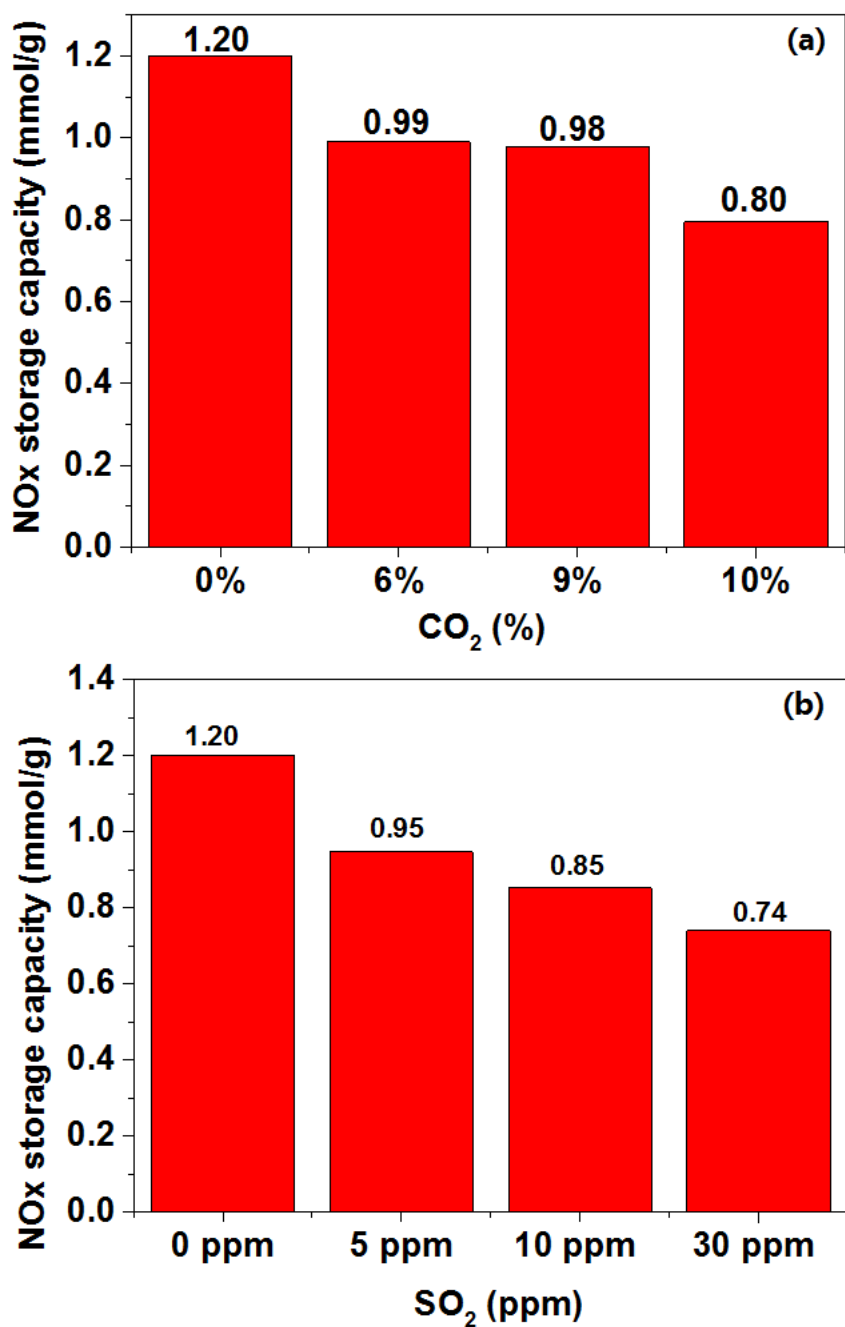


**Fig. 11.** (a) The effect of CO<sub>2</sub> on the NO<sub>x</sub> storage capacity of 1 wt% Pt-15 wt% K<sub>2</sub>CO<sub>3</sub>/Co<sub>1</sub>Mg<sub>2</sub>Al<sub>1</sub>O<sub>x</sub> at 300 °C. Feed: 100 ppm NO<sub>x</sub>, 6–9% CO<sub>2</sub>, 10% O<sub>2</sub> with Ar balance, 300 mL/min. (b) The effect of SO<sub>2</sub> on the NO<sub>x</sub> storage capacity of 1 wt% Pt-15 wt% K<sub>2</sub>CO<sub>3</sub>/Co<sub>1</sub>Mg<sub>2</sub>Al<sub>1</sub>O<sub>x</sub> at 300 °C. Feed: 100 ppm NO<sub>x</sub>, 5–30 ppm SO<sub>2</sub>, 10% O<sub>2</sub> with Ar balance, 300 mL/min.